Title

Role of Nonequilibrium Water Vapor Diffusion in Thermal Energy Storage Systems in the Vadose Zone

Journal

Journal of Geotechnical and Geoenvironmental Engineering, 144(7)

ISSN

1090-0241

Authors

Başer, T
Dong, Y
Moradi, AM
et al.

Publication Date

2018-07-01

DOI

10.1061/(asce)gt.1943-5606.0001910

Peer reviewed

ROLE OF NONEQUILIBRIUM WATER VAPOR DIFFUSION IN GEOTHERMAL ENERGY STORAGE SYSTEMS IN THE VADOSE ZONE

by T. Başer, Ph.D., S.M.ASCE[1], Y. Dong, Ph.D., A.M.ASCE[2], A.M. Moradi, Ph.D.[3], N. Lu, Ph.D., F.ASCE[4], K. Smits, Ph.D.[5], S. Ge, Ph.D.[6], D. Tartakovsky, Ph.D.[7], and J.S. McCartney, Ph.D., P.E., M.ASCE[8]

Abstract: Although siting of geothermal energy storage systems in the vadose zone may be beneficial due to the low heat losses associated with the low thermal conductivity of unsaturated soils, water phase change and vapor diffusion in soils surrounding geothermal heat exchangers may play important roles in both the heat injection and retention processes that are not considered in established design models for these systems. This study incorporates recently-developed coupled thermo-hydraulic constitutive relationships for unsaturated soils into a coupled heat transfer and water flow model that considers time-dependent, nonequilibrium water phase change and enhanced vapor diffusion to study the behavior of geothermal energy storage systems in the vadose zone. After calibration of key parameters using a tank-scale heating test on compacted silt, the ground response during 90 days of heat injection from a vertical geothermal heat exchanger

[1] Research Associate, University of Alberta, Dept. of Civil and Environmental Engineering, 9211 - 116 Street NW Edmonton, Alberta, Canada T6G 1H9. tugce@ualberta.ca.
[2] Associate Professor, State Key Laboratory of Geomechanics and Geotechnical Engineering, Institute of Rock and Soil Mechanics, Chinese Academy of Sciences, Wuhan, Hubei 430071, P.R. China. ydong@whrsm.ac.cn.
[3] Research Associate, Center for Experimental Study of Subsurface Environmental Processes (CESEP), Colorado School of Mines, Dept. of Civil and Environmental Engineering, 1500 Illinois St., Golden, CO 80401. amoradig@mines.edu.
[4] Professor, Colorado School of Mines, Dept. of Civil and Environmental Engineering, 1500 Illinois St., Golden, CO 80401. ninglu@mines.edu.
[5] Assistant Professor, Center for Experimental Study of Subsurface Environmental Processes (CESEP), Colorado School of Mines, Dept. of Civil and Environmental Engineering, 1500 Illinois St., Golden, CO 80401. ksmits@mines.edu.
[6]Professor, University of Colorado Boulder, Dept. of Geosciences. Boulder, CO 80309-0399. Shemin.Ge@colorado.edu.
[7] Professor, Stanford University, Dept. of Energy Resources Engineering, 367 Panama St., Stanford, CA 94305. tartakovsky@stanford.edu.
[8] Associate Professor, University of California San Diego, Dept. of Structural Engineering. 9500 Gilman Dr., La Jolla, CA 92093-0085, mccartney@ucsd.edu.

followed by 90 days of ambient cooling was investigated. Significant decreases in degree of saturation and thermal conductivity of the ground surrounding the vertical geothermal heat exchanger were observed during the heat injection period that were not recovered during the cooling period. This effect can lead to a greater amount of heat retained in the ground beyond that estimated in conduction-based design models.

INTRODUCTION

An important challenge facing society is the storage of energy collected from renewable sources. One such application is the storage of heat collected from solar thermal panels in the subsurface so that it can be harvested later (Claesson and Hellström 1981; Nordell and Hellström 2000; Chapuis and Bernier 2009). A practical mode of heat injection into the subsurface involves circulation of a heated carrier fluid through a closely-spaced array of closed-loop geothermal heat exchangers in boreholes to reach ground temperatures ranging from 35 to 80 °C (Sibbitt et al. 2012; Başer et al. 2016a; McCartney et al. 2017). Unsaturated soils in the vadose zone are ideal thermal energy storage media because low heat losses can be expected due to the low thermal conductivity of unsaturated soils (McCartney et al. 2013). The mode of heat transfer during injection of heat into unsaturated soils is complex as it may be coupled with thermally-induced water flow in either liquid or vapor forms along with latent heat transfer associated with phase change. However, most design models for geothermal heat storage systems focus on ground temperature changes during heating and do not consider coupled heat transfer and water transport (Claesson and Hellström 1981; Eskilson 1987). Although some recent studies on geothermal energy storage systems highlighted the importance of considering coupled heat transfer and water flow in their performance evaluation (Catolico et al. 2016; Moradi et al. 2016), the impact of water vapor diffusion and phase change in unsaturated soils during heat injection on the heat retention

during a subsequent ambient cooling phase is an important topic that has not been investigated. This paper presents simulations of the response of a low-permeability, low activity, incompressible, unsaturated silt layer surrounding a single geothermal heat exchanger to understand the impacts of considering water vapor diffusion and water phase change on the transient heat injection and retention processes. Comparison of the simulation results from the coupled heat transfer and water flow model with a simpler heat transfer model without water vapor diffusion or phase change permits an evaluation of the importance of these heat transfer mechanisms in simulating geothermal energy storage systems in the vadose zone.

BACKGROUND

Most models of heat transfer from geothermal heat exchangers employ analytical solutions to the heat equation assuming conduction is the primary mechanism of heat transfer, using constant thermal properties that do not consider the effects of changes in degree of saturation expected during heat transfer in unsaturated soils (e.g., Kavanaugh 1985; Eskilson 1987). Analytical solutions have been developed for geothermal heat exchanger geometries including the infinite line source (Ingersoll and Plass 1948; Beier et al. 2014), finite line source (Acuña et al. 2012; Lamarche and Beauchamp 2007), hollow cylinder source (Ingersoll et al. 1954; Gehlin 2002), finite plate source (Ciriello et al. 2015), and one- and two-dimensional solid cylinder sources (Tarn and Wang 2004). Although numerical simulations of geothermal heat exchangers have also been performed, most have also considered conduction as the primary mechanism of heat transfer (Ozudogru et al. 2015; Welsch et al. 2015; Başer et al. 2016a). While these conduction-based analytical models and numerical simulations may be practical for the design of geothermal heat exchangers in dry or saturated low permeability soils, they may not be practical for design of those in unsaturated soils due to the potential for convective heat transfer associated with thermally-

induced liquid water or water vapor flow, which may result in irreversible changes in behavior during cyclic heat injection and extraction (or ambient cooling). Further, the thermal properties of unsaturated soils are highly dependent on the degree of saturation, even when conduction is assumed to be the primary mode of heat transfer (e.g., Farouki 1981; Côté and Konrad 2005; Smits et al. 2013; Lu and Dong 2015). Conduction-only models may also not be practical for use in saturated soils with high permeability due to the potential for thermally-induced convection of water from buoyancy effects (Catolico et al. 2016).

Because the properties of water in liquid and gas forms are dependent on temperature, heat transfer in the unsaturated soils in the vadose zone leads to thermally induced water flow through soil. Specifically, temperature dependency of the density of liquid water ρ_w (Hillel 1980), dynamic viscosity of liquid water μ_w (Lide 2001), surface tension of soil water σ (Saito et al. 2006), relative humidity at equilibrium $R_{h,eq}$ (Philip and de Vries 1957), saturated vapor concentration in the gas phase $c_{v,sat}$ (Campbell 1985), vapor diffusion coefficient in air D_v (Campbell 1985), and the latent heat of water vaporization L_w (Monteith and Unworth 1990) may lead to thermally-induced water flow through unsaturated soils. The movement of water in soil caused by thermal and hydraulic gradients and the associated impacts on heat transfer have been studied experimentally for more than 100 years (Bouyoucos 1915; Lewis 1937; Smith 1943; Gurr et al. 1952; Baladi et al. 1981; Shah et al. 1983; Ewen 1988; Gens et al. 1998, 2007, 2009; Cleall et al. 2011; Smits et al. 2011; Moradi et al. 2015, 2016; Başer et al. 2016b). Some general observations from these studies are: (1) heat transfer occurs in unsaturated porous media by conduction, convection in both liquid and gas phases, and latent heat transfer associated with water phase change; (2) water movement due to a temperature gradient is controlled by both vaporization/condensation processes as well as development of suction gradients caused by changes in water properties with temperature (i.e.,

density, viscosity, solid-liquid contact angle) and drying effects; (3) vapor diffusion may occur at greater rates than predicted by Fick's law, (4) the magnitude of thermally induced water flow depends on the initial degree of saturation; and (5) the times required to reach steady-state distributions in degree of saturation and temperature may be different depending on the coupling between the thermal and hydraulic properties of a given soil.

The governing equations for coupled heat transfer and flow of water in liquid and vapor forms have been investigated for unsaturated porous media in nondeformable conditions (Philip and de Vries 1957; Ewen and Thomas 1989; Thomas and King 1991; Thomas and Sansom 1995; Thomas et al. 2001; Smits et al. 2011), deformable conditions (Thomas and He 1996; Thomas et al. 1996), and in the presence of pore fluids containing salts or chemicals (Cleall et al. 2007; Olivella et al. 1996; Guimaraes et al. 2007, 2013). Most models for coupled heat transfer and water flow in liquid and vapor forms in nondeformable unsaturated soils are based on the model of Philip and de Vries (1957), who proposed the "liquid island" theory as an explanation for observations from studies like Gurr et al. (1952) that vapor diffusion occurred at a faster rate than predicted by Fick's law. Their theory is a pore-scale explanation where local thermal gradients is assumed to be higher across microscopic air-filled pores than the global thermal gradient across a soil element, and where water vapor diffusion is enhanced by evaporation and condensation from water held between soil particles by capillarity (liquid islands), effectively increasing the area available for vapor diffusion through a soil element. They implemented their pore-scale theory on a macroscopic scale by extending the vapor diffusion theory of Penman (1940) through inclusion of a soil-specific enhancement factor to correct the vapor diffusion rate calculated from Fick's law. Cass et al. (1984) found that the enhancement factor approaches 1.0 (no enhancement) for dry soils and increases significantly with increasing degree of saturation. Although the model of Philip and

de Vries (1957) has been used in many coupled heat transfer and water flow problems in nondeformable soils, their model does not account for convective transport in the gas or liquid water phases, nonequilibrium phase change, vapor dispersion, or sensible heat dispersion in the liquid phase (Smits et al. 2011). Of these issues, consideration of nonequilibrium phase change in the model is expected to lead to more accurate identification of the appropriate vapor enhancement factor for a given soil (Smits et al. 2011). Lozano et al. (2008) observed that phase change may become the process limiting evaporation at low saturations rather than vapor diffusion as classically believed.

In the model of Philip and de Vries (1957), it is assumed that the water in liquid and gas phases are in equilibrium, which means that phase change occurs instantaneously in response to a change in vapor pressure. However, experimental studies have identified that time is required for liquid water to volatilize in response to a change in vapor pressure in a pore resulting from vapor diffusion in response to gradients in vapor pressure and/or temperature (Bénet and Jouanna 1982; Armstrong et al. 1994; Chammari et al. 2008, Bénet et al. 2009). To account for this in a model of coupled heat transfer and water flow, a source term for the liquid/gas phase change rate is added to the mass balance equations of liquid and vapor that is based on irreversible thermodynamics, first order reaction kinetics, or the kinetic theory of gases and contains a fitting coefficient that can calibrated for a given soil (Bénet and Jouanna 1982; Bixler 1985; Zhang and Datta 2004). Smits et al. (2011) adopted the source term of Bixler (1985) because it was derived from the kinetic theory of gases and is thus inherently temperature dependent. In the model of Bixler (1985), the vaporization rate is proportional to the difference between local equilibrium vapor pressure and local partial vapor pressure and the difference between the local degree of saturation and residual saturation. Smits et al. (2011) compared predictions of coupled heat transfer and water flow from

equilibrium and nonequilibrium models, and found major differences in the early stages of the flow process, with greater differences for soils with initially lower degrees of saturation. Smits et al. (2011) and Trautz et al. (2015) also found that nonequilibrium models provide a better match to experimental data from column tests involving evaporation from fine sand with a heated surface than the model of Philip and de Vries (1957), indicating that the nonequilibrium assumption for phase change may better capture the transient process of thermally-induced drying.

MODEL CALIBRATION

Model Description

A non-equilibrium, non-isothermal, and coupled heat transfer and water flow numerical model developed by Smits et al. (2011) and extended by Moradi et al. (2016) was used to consider the behavior of an unsaturated soil layer during heating and cooling of a single vertical geothermal heat exchanger. The governing equations and primary variables used in the formulation are given in Table 1. Calibration of the model requires soil-specific quantification of the parameters for the thermo-hydraulic constitutive relationships governing water retention, hydraulic conductivity, thermal conductivity, and volumetric heat capacity, as well as estimates of parameters a and b in Equations (4) and (5) that govern the rates of vapor diffusion and phase change, respectively.

The model used in the simulations incorporates recently-developed thermo-hydraulic constitutive relationships for unsaturated soils (Lu and Dong 2015; Baser et al. 2016c). The experimental approach used by Lu and Dong (2015) was used to obtain the data for calibration of these coupled thermo-hydraulic constitutive relationships. Lu and Dong (2015) used a modified form of the transient-release and imbibition method (TRIM) of Wayllace and Lu (2012) that included a dual-needle thermal probe to measure the thermal conductivity and volumetric heat capacity during monotonic drying of different unsaturated soils under isothermal conditions.

154 TRIM uses an inverse analysis to estimate the parameters of the soil-water retention curve (SWRC)
155 and hydraulic conductivity function (HCF) given by van Genuchten (1980). These parameters
156 include α_{vG}, which represents the inverse of the air entry suction in the SWRC, N_{vG}, which
157 represents the pore size distribution in the SWRC, and k_{sw}, which is the hydraulic conductivity of
158 saturated soil. The value of k_{sw} obtained from a test at room temperature can be used to calculate
159 the intrinsic permeability κ in Equation (1). Although the saturation-dependent relative
160 permeability to water (the HCF) was assumed not to vary with temperature, the hydraulic
161 conductivity of the unsaturated soil will vary with temperature because the dynamic viscosity and
162 density of water vary with temperature according to the relationships presented in Lide (2001) and
163 Hillel (1980), respectively. The relative permeability to gas was not measured in this study, but
164 was assumed to equal $k_{rg}=1-k_{rw}$. The temperature-dependent surface tension σ relationship
165 presented by Saito et al. (2006) was used in the temperature correction for capillary pressure of
166 Grant and Salehzadeh (1996), given as follows:

$$P_c(T) = P_c(T_{ref})[\sigma(T)/\sigma(T_{ref})] \quad (7)$$

167 where σ is the surface tension (N/m), T is the temperature (K), and T_{ref} is the initial reference
168 temperature of 293.15 K.

169 Lu and Dong (2015) defined a thermal conductivity function (TCF) that can capture transitions
170 in the thermal conductivity in the capillary, funicular, and pendular water retention regimes of the
171 SWRC, given as follows:

$$\frac{\lambda - \lambda_{dry}}{\lambda_{sat} - \lambda_{dry}} = 1 - \left[1 + \left(\frac{S_{rw}}{S_f}\right)^m\right]^{1/m-1} \quad (8)$$

172 where λ_{dry} and λ_{sat} are the thermal conductivities of dry and saturated soil specimens, respectively,
173 S_f is a parameter representing the degree of saturation at the onset of the funicular regime, and m

is a parameter related to the pore fluid network connectivity. Lu and Dong (2015) correlated the parameters of the TCFs and SWRCs of several soils and found that the *m* parameter in the TCF is related to the pore-size parameter N_{vG} in the SWRC model of van Genuchten (1980), and can be estimated to be $3.0\text{-}0.2N_{vG}$. Evaluation of the form of Equation 8 indicates that the thermal conductivity will not reduce to the value of λ_{sat} when $S_e=1$, so Lu and Dong (2015) treated λ_{sat} as a fitting parameter. Although Smits et al. (2013) observed that the TCF may vary with temperature, this temperature dependency is likely due to vapor diffusion and phase change that was not accounted for in their simulations. Because the simulations in this study account for vapor diffusion and phase change explicitly, the TCF and VCHF measured at 20 °C were used in the coupled heat transfer and water flow simulations.

Başer et al. (2016c) presented trends in the volumetric heat capacity of compacted silt during monotonic drying and found that it also depends on the degree of saturation in a similar manner to the thermal conductivity, and defined a volumetric heat capacity function (VCHF) that has the same form as the THF of Lu and Dong (2015), as follows:

$$\frac{C_v - C_{v\,\mathrm{dry}}}{C_{v\,\mathrm{sat}} - C_{v\,\mathrm{dry}}} = 1 - \left[1 + \left(\frac{S_{rw}}{S_{\mathrm{f}}}\right)^{m}\right]^{1/m-1} \tag{9}$$

where C_{vdry} and C_{vsat} are the volumetric heat capacities of dry and saturated soil, respectively, and are similarly treated as fitting parameters, and S_f and *m* are the same parameters as in Equation (8). Başer et al. (2016c) found that this model and the assumptions regarding the parameters provided a good match to the volumetric heat capacity data measured in the TRIM tests on different soils performed by Lu and Dong (2015) that were not reported in their paper due to its focus on the thermal conductivity.

Calibration of Thermo-Hydraulic Constitutive Relationships

The soil investigated in this study is Bonny silt, which is classified as ML (inorganic silt) according to the Unified Soil Classification System (USCS), and has a specific gravity of 2.65. Silt was selected for this evaluation because it is not expected to deform significantly during changes in temperature or degree of saturation, and its low activity of 0.33 (plasticity index of 4 divided by clay size fraction of 12%) indicates that it will not have significant diffuse double layer effects which could complicate thermo-hydraulic analyses. The silt specimens used in the calibration process were prepared using compaction at a gravimetric water content of 13.7% to a dry unit weight of 14.0 kN/m^3, which correspond to an initial degree of saturation of 0.42 and a porosity of 0.46. For reference, the optimum water content and the maximum dry unit weight corresponding to the standard Proctor compaction effort are 13.6% and 16.3 kN/m^3 respectively.

The SWRC and HCF (in terms of the relative permeability to water) obtained from the modified TRIM test on compacted Bonny silt are shown in Figure 1(a) along with the model parameters. The shape of the SWRC indicates that an appreciable amount of water will be retained in the soil several meters above the water table under hydrostatic conditions. The compaction conditions for these curves are the same as those mentioned above, even though Lu and Dong (2015) report a different porosity due to a lower value of G_s used in their calculations. An intrinsic permeability of 1.27×10^{-14} m^2 was calculated from the hydraulic conductivity of saturated soil of 1.24×10^{-7} m/s and the values of water viscosity and density at 20 °C (293.15 K). The TCF and VHCF for Bonny silt are shown in Figure 1(b), along with the TCF and VHCF parameters in Equations (8) and (9). The value of m = 2.62 measured in the experiment for Bonny silt was used in the simulations, which is lower than the value of 2.68 obtained from the correlation between m and N_{vG} of Lu and Dong (2015). The experimental value still reflects the coupling between the

thermo-hydraulic properties as they were defined in the same test. The thermal conductivity ranges from 1.25 to 0.37 W/mK for saturated to dry conditions, respectively, while the volumetric heat capacity ranges from 2.75 to 1.30 MJ/m^3K for saturated to dry conditions, respectively. The variations in these parameters with degree of saturation indicate that changes in heat retention within a storage volume may occur if a soil experiences drying during heat injection.

Calibration of Vapor Diffusion and Phase Change Parameters

To define the parameters *a* and *b*, a tank-scale heat injection experiment was performed in an instrumented layer of compacted Bonny silt, which was then simulated using the parameters from the thermo-hydraulic constitutive relationships defined in Figure 1. A schematic of the experimental setup is shown in Figure 2. Bonny silt was compacted in 9 lifts in a cylindrical aluminum container having a diameter of 550 mm and a height of 477 mm. A 215 mm-long cylindrical cartridge heater having a diameter of 10 mm was used as the heating source. During heat injection, a temperature control unit was used to impose a constant temperature boundary condition of 60 °C on the heating rod. To monitor changes in temperature and degree of saturation during heating of the soil, ten 5TM dielectric sensors manufactured by Decagon Devices of Pullman, WA were placed at the locations shown in Figure 2. After all the lifts and sensors were placed, the top of the soil layer was covered with several layers of plastic wrap to minimize loss of water vapor to the laboratory air. The top and sides of the tank were then wrapped in insulation, and thermocouples were used to monitor the temperatures of the boundaries of the tank. The soil had an initial temperature of 23.5 °C and an initial degree of saturation of 0.42.

In the simulations of the tank-scale tests, no mass flux boundary conditions were applied for both liquid water and vapor flow for all boundaries of the tank. The top boundary was thermally insulated, convective heat flux boundaries were defined for the side boundaries to consider heat loss from the tank, a constant temperature boundary condition was used for the heating rod, and a

constant temperature of 18 °C was applied at the bottom of tank. The system of partial differential equations in Table 1 was solved simultaneously using COMSOL Multiphysics software. Results from the numerical analyses were then compared with the experimental results to calibrate the parameters *a* and *b*. Comparisons of predicted and measured time series of temperature and degree of saturation inferred from dielectric sensor #3 are shown in Figures 3(a) to 3(d). Sensor #3 was selected as the primary location for calibration of the model as it is near the center of the heating rod and is relatively close to the heat exchanger. The predicted time series in these figures include curves for different values of the fitting parameters *a* and *b*. The parameters are observed to have a greater effect on the change in degree of saturation as they control the rates of vapor diffusion and water phase change. Simulations from a model where no vapor diffusion or phase change is considered (hereafter referred to as the "no vapor" case) are also shown in Figures 3(a) and 3(b), which indicate slower increases in temperature to lower magnitudes at this location as well as a negligible change in degree of saturation. Values of $a = 30$ and $b = 5\times10^{-7}$ s/m^2 were found to best fit the Bonny silt data based on visual inspection, a similar approach used by Smits et al. (2011).

To evaluate the calibration, the spatial distributions of temperature and degree of saturation along Transects B and A at the end of the heating from the numerical simulations and the experiments are shown in Figures 4(a) through 4(d). In most of the cases, the predicted profiles show good agreement with the measured data, except in the case of the degree of saturation measured by the sensor nearest the edge of container in Figure 4(b). This sensor may have malfunctioned due to the compaction process. Overall, the comparisons between model predictions and experimental results in Figures 3 and 4 indicate that the calibrated values of *a* and *b* can be assumed to be representative of Bonny silt under these compaction conditions.

EVALUATION OF VAPOR DIFFUSION AND PHASE CHANGE AROUND A FIELD-SCALE GEOTHERMAL HEAT EXCHANGER

Scenario Considered

The main goal of this study is to use the calibrated parameters to understand the changes in the behavior of a layer of unsaturated Bonny silt surrounding a geothermal heat exchanger during a heating and cooling cycle representative of geothermal energy storage systems. Although geothermal heat storage systems typically involve an array of geothermal heat exchangers with spacings as close at 1.5 m (Baser et al. 2016a), this study focuses on the changes in soil behavior around a single geothermal heat exchanger. This choice simplifies the boundary conditions and permits evaluation of the relative effects of the different heat transfer mechanisms. It is possible that the close spacing between geothermal heat exchangers may lead to different distributions in temperature and degree of saturation than those observed in this evaluation due to interactions between heat exchangers, but the simpler scenario of a single vertical geothermal heat exchanger is evaluated in this paper to help establish the impact of a heating-cooling cycle on the distributions in temperature and degree of saturation in the surrounding unsaturated silt layer.

The vertical geothermal heat exchanger investigated in this study has a length of 25 m and a radius of 0.04 m, embedded at a depth of 1 m from the surface. The embedment is consistent with the practice of installing geothermal heat exchangers below the frost depth. Even though this scenario could be investigated using an axisymmetric analysis, a 3D simulation was performed for a rectangular domain so that the domain could be modified to incorporate additional geothermal heat exchangers in future studies. The quarter domain having a height of 30 m and a width of 10 m with the geothermal heat exchanger along one edge is shown in Figure 5. The entire domain was assumed to be uniform and isotropic, and the soil was discretized into 101,073 elements (394,394

287 degrees of freedom) with finer elements around the heat exchanger. The hydraulic and thermal
288 boundary conditions for the models are also shown in Figure 5. For liquid water and gas flow,
289 Neumann boundary conditions (no mass flux) were assumed for all boundaries except the bottom
290 boundary, which was set to be a constant head boundary condition corresponding to the water
291 table. For heat transfer, a constant temperature that represents an average mean subsurface soil
292 temperature of 21 °C was applied at the bottom while at the outer boundaries the temperature
293 varied with depth. No flux boundary conditions were applied to the planes of symmetry. The size
294 of the domain was selected to be large enough that a constant temperature and zero fluid flux could
295 be assumed on the outer vertical boundaries.

296 The initial conditions are shown in the color bars in Figure 5. The initial ambient temperature
297 of the domain was assumed to be a function of depth until a certain depth of 9 m from surface, and
298 this initial temperature profile is a representative of early summer months in San Diego
299 (specifically May 2015). A hydrostatic initial condition was assumed, so the soil along the length
300 of the heat exchanger is unsaturated with initial degrees of saturation ranging from 0.50 to 0.21
301 depending on the height from the water table. Two locations of interest that will be investigated
302 further are noted in Figure 5(b) having different initial degrees of saturation.

303 During heat injection, a constant heat flux of 50 W/m^2 was applied to the outer boundary of
304 the geothermal heat exchanger. This heat flux was converted to a volumetric heat source to obtain
305 the value of Q in Equation (6). Although the magnitude of heat flux used in this study is
306 representative of average value in geothermal energy storage systems (Acuña et al. 2012; Welsch
307 et al. 2015; McCartney et al. 2017), a constant heat flux is not expected in a system where solar
308 thermal panels are the heat source. In these cases, the input temperature from the solar thermal
309 panels will remain relatively constant, which means that the heat flux will decrease with time as

the subsurface warms (Welsch et al. 2015). Although use of a constant heat flux will lead to greater increases in ground temperature than those expected when using solar thermal panels as the heat source, it provides a simple boundary condition for evaluating the roles of different heat transfer mechanisms in unsaturated soils.

Heat Transfer and Water Flow Evaluation

The temperature time series at a distance of 0.05 m from the geothermal heat exchanger and a depth of 8.5 m from the surface (i.e., S_{r0} = 0.25) is shown in Figure 6(a). After the 90-day heat injection period, the ground temperature reached a maximum value of 45.6 °C at this location. For comparison, the temperature time series from the model where no vapor diffusion or phase change is considered (the no vapor case) is also shown in Figure 6(a). In addition to showing a slower rate of increase in temperature, a lower maximum temperature of 36.3 °C was observed for the no vapor case. After the heating injection period, the heat flux was set to 0 W/m^2 and the soil was allowed to cool ambiently. After 180 days from the start of the simulation (90 days after the end of heat injection), the temperature decreased to 22.8 °C for the model with vapor diffusion and phase change and to 21.8 °C for the no vapor case. Although the gradients for heat loss are higher in the model with vapor diffusion and phase change, more heat is retained at this location after the 180-day cooling period due to the decrease in degree of saturation of the soil during heat injection due to vapor diffusion and latent heat transfer observed in Figure 6(b). Specifically, at the end of the heat injection period, a decrease in degree of saturation of 0.14 at this depth was observed for the model with vapor diffusion and phase change, while a negligible decrease in degree of saturation of 0.01 was observed for the no vapor case. The greater decrease in the degree of saturation for the model with vapor diffusion and phase change led to a decrease in thermal conductivity according to the TCF (from 0.84 to 0.49 W/mK), which will be assessed in more

detail later. Another interesting observation from Figure 6(b) is that at the end of the 90-day cooling period, only 16.5% of the decrease in degree of saturation observed during heat injection was recovered, indicating that the drying near the heat exchanger was permanent from a practical point of view. This may have an impact on subsequent heat injection and cooling cycles, and may be one of the reasons that an increase in the ground temperature is observed after several cycles of heat injection and extraction in practice (Sibbitt et al. 2012).

Radial distributions in temperature at a depth of 8.5 m from the surface at the ends of the heat injection and cooling periods are shown in Figure 7(a). Heat injection led to a notable change in temperature up to a distance of about 3 m from the heat exchanger. The temperature at the location of the heat exchanger was nearly 10 °C greater when vapor diffusion and latent heat transfer was considered than the case when it was not, and the temperature at the end of the ambient cooling period was greater throughout the zone of influence. A decrease in degree of saturation was only observed within approximately 1 m from heat exchanger for the model with vapor diffusion and phase change, as shown in Figure 7(b). A slight decrease in degree of saturation was observed near the heat exchanger for the no vapor case due to thermally-induced liquid flow. The zone of influence for temperature changes is greater than the zone of influence for degree of saturation changes for the conditions evaluated. For Bonny silt, this indicates that an overlap in the effects of different heat exchangers may be observed for the typical geothermal heat exchanger spacing of 1.5 m in geothermal energy storage systems.

Profiles of temperature with depth at horizontal distances of 0.05 m and 0.20 m from the heat exchanger at the end the 90-day heat injection period are shown in Figure 8(a). The temperature profiles varied nonlinearly with depth and had a maximum value at a depth of 4.5 m from the surface. For comparison, the temperature profiles for the no vapor case show more uniform

distributions in temperature with depth at the end of the heat injection period. The difference in temperature observed with depth in both models is due to the thermo-hydraulic properties with depth associated with the variations in initial degree of saturation with depth shown in Figure 5. A significant decrease in the in degree of saturation with depth is observed at both horizontal distances for the model with vapor diffusion and phase change in Figure 8(b), while only a slight decrease was observed for the no vapor case. Profiles of temperature after the ambient cooling are shown in Figure 8(c), with the profiles at horizontal distances of 0.05 m and 0.20 m overlapping. Although most of the heat injected has dissipated away from the heat exchanger, a greater amount of heat was retained in the soil close to the heat exchanger for the model with vapor diffusion and phase change. The profiles of degree of saturation at the end of the cooling period shown in Figure 8(d) only show slight increases from the profiles observed in Figure 8(b).

The impact of the initial degree of saturation on heat transfer and water flow can be investigated by evaluating the transient response at different depths in the soil profile, which have different initial degrees of saturation. Time series of temperature at depths of 8.5 m and 24.5 m from the surface at a horizontal distance of 0.05 m from the heat exchanger corresponding to initial degrees of saturation of 0.25 and 0.50 are shown in Figure 9(a). Increases in temperature of 45.6 and 42.3 °C at the end of the heat injection period were observed when the initial degree of saturation was doubled from 0.25 to 0.50. However, decreases in degree of saturation of 0.14 and 0.35 were observed at the end of the heat injection period for the same depths, as shown in Figure 9(b). The greater decrease in degree of saturation for the initially wetter soil is likely due to the availability of water to evaporate from the region near the heat exchanger. The horizontal zone of influence of the change in temperature is similar for the two depths as shown in Figure 9(c), but the horizontal zone of influence of the change in degree of saturation was greater at the depth of 8.5 m as shown

379 in Figure 9(d). This is consistent with observations that dryer initial conditions lead to greater
380 zones of influence of vapor diffusion (e.g., Smits et al. 2011). The soil with S_{r0}=0.50 also shows a
381 slight wetting front due to the movement of water away from the heat exchanger.

382 **Assessment of Heat Transfer Mechanisms and Effects of Coupled Flow**

383 Profiles of thermal conductivity and volumetric heat capacity that correspond to the profiles of
384 degree of saturation in Figure 8(b) are shown in Figures 10(a) and 10(b), respectively. Despite the
385 nonlinear decrease in degree of saturation along the length of the heat exchanger, a comparatively
386 uniform decrease of approximately 0.3 W/mK is observed at 0.05 m from the heat exchanger. A
387 more nonlinear decrease in thermal conductivity is observed further away from the heat exchanger
388 at 0.20 m. The shapes of the profiles of the volumetric heat capacity are the same as those for the
389 thermal conductivity due to the same parameters used in Equations (8) and (9), but because of the
390 range of the two relationships for Bonny silt the volumetric heat capacity decreased by as much as
391 25% while the thermal conductivity decreased by as much as 70%. This is a positive finding for
392 geothermal energy storage in similar soil deposits, as it means that lower heat losses can be
393 expected without a significant reduction in the quantity of heat stored.

394 The vapor diffusion and latent heat transfer that results in the drying around the heat exchanger
395 also leads to a suction gradient that may result in liquid water flow back toward the heat exchanger.
396 Horizontal profiles of suction profiles at a depth of 8.5 m (S_{r0}=0.25) at different times are shown
397 in figure 11(a). Large increases in suction are observed within 0.6 m from the heat exchanger, with
398 decreases in suction beyond that point. Despite the large gradient associated with the suction
399 distribution at the end of the heating period, the suction did not return to its original distribution
400 during the ambient cooling period. This may have been due to the order of magnitude decrease in

401 the hydraulic conductivity (adjusted for temperature effects) shown in Figure 11(b), indicating that
402 more time may be needed for liquid flow to occur than permitted in the 90-day cooling period.
403 Vapor concentrations (kg/m^3) near the heat exchanger normalized by the equilibrium vapor
404 concentration (kg/m^3) are shown in Figure 12(a) for Bonny silt with initial degrees of saturation
405 of 0.25 and 0.50 (depths of 8.5 and 24.5 m). When the normalized vapor concentration is greater
406 or equal to 0.75, the phase change in the soil can be assumed to be near equilibrium (Lozano et al.
407 2008). For an initial degree of saturation of 0.25, the normalized vapor concentration soon after
408 the start of heating was smaller than this limit. The normalized vapor concentration decreased to
409 0.63 at the end of the heating period, indicating that use of the nonequilibrium model was justified.
410 For an initial degree of saturation of 0.5, the normalized vapor concentration was 0.82 soon after
411 the start of heating and remained above 0.75 indicating that an equilibrium phase change
412 assumption may be valid for initially wetter soils. The time series in Figure 12(a) indicate that the
413 phase change process did not reach steady state conditions by the end of the heat injection period.
414 Horizontal profiles of the normalized vapor concentrations at the end of heating shown in Figure
415 12(b) indicate that lower vapor concentrations were present near the heat source and had a similar
416 zone of influence to the degree of saturation in Figure 7(b). Despite the higher magnitudes of
417 normalized vapor concentration, greater changes in normalized vapor concentration with
418 horizontal distance are observed for the initially wetter soil (S_{r0}=0.5), which may be the reason for
419 the greater change in degree of saturation at this location. Vertical profiles of normalized vapor
420 concentration at the end in Figure 12(c) are similar to those for the degree of saturation in Figure
421 8(b). A higher vapor concentration was observed close to the surface because of the lower initial
422 degrees of saturation and higher temperatures and because of upward movement of water vapor
423 due to buoyancy effects.

Horizontal profiles of the latent heat transfer rate, calculated as the product of $L_w R_{gw}$ in Equation (6), at the end of heat injection for soil at depths corresponding to initial degrees of saturation of 0.25 and 0.50 are shown in Figure 13(a). While a positive latent heat transfer rate was higher near the heat source indicating evaporation, a very slight value less than zero was observed at a distance about 1 m away from the heat exchanger. This indicates that condensation is occurring in the soil at lower temperatures further from the heat source. A comparison between the total thermal energy injected into the geothermal heat exchanger and the total latent heat (i.e., the total energy associated with phase change calculated by integrating the product of $L_w R_{gw}$ over the volume of the domain and over time) is shown in Figure 13(b). The total energy associated with phase change at the end of 90 days was 44 MJ, which is approximately 24% of the total heat injected into the system of 180 MJ. This indicates that an appreciable amount of the thermal energy injected into the system leads to phase change and further justifies the need to accurately account for nonequilibrium phase change effects in unsaturated soils. The total latent heat appears to have stabilized over the heat injection period, which may be because of the decrease in degree of saturation and reduction in availability of water to change phase near the heat exchanger.

CONCLUSIONS

A model that includes a recently-developed set of thermo-hydraulic constitutive relationships was used to understand the roles of vapor diffusion and phase change on the coupled heat transfer and water flow in a fine-grained, non-deformable unsaturated silt layer initially under hydrostatic conditions surrounding a vertical geothermal heat exchanger during heat injection and ambient cooling. In general, the modeling results confirm the importance of considering vapor diffusion and water phase change in simulations of geothermal heat exchangers in unsaturated soils, as well as the relevance of considering nonequilibrium phase change in initially drier soil layers. Although

quantitative conclusions from the simulations are specific to the given soil and geometry investigated, several conclusions can be drawn regarding the use of geothermal heat exchangers in geothermal energy storage systems in unsaturated soils, including:

- A greater rate of increase in temperature and greater magnitude of temperature change were observed in the soil near the heat exchanger during heat injection in a model that includes enhanced vapor diffusion and phase change. This conclusion indicates that conduction-only design models may underestimate the heat injection response of geothermal energy storage systems in the vadose zone.
- The heat retained in the soil near the heat exchanger during an ambient cooling period was greater when considering vapor diffusion and phase change, despite the greater thermal gradient compared to a model with no vapor. This was found to be due to the decrease in thermal conductivity associated with drying during heat injection. The drying during heat injection can be considered permanent for practical purposes within the time frame of ambient cooling considered. This may partially be due to the decrease in hydraulic conductivity due to thermally-induced drying, leading to a negligible amount of liquid water flow back toward the heat exchanger during ambient cooling.
- Although reductions in both thermal conductivity and volumetric heat capacity are observed during thermally induced drying of the soil near the geothermal heat exchanger, the percentage reductions in thermal conductivity were greater. This indicates that the greater amount of heat retention can be expected in unsaturated soils during ambient cooling, but the maximum possible heat stored will not decrease by as large of an amount.
- The zone of influence of changes in temperature was observed to be greater than the zone of influence of changes in degree of saturation for the silt under investigation, but both zones of

influence are appreciable enough that overlap is expected in geothermal energy storage systems with closely-spaced geothermal heat exchangers (i.e., 1.5 to 2.0 m).

- The normalized vapor concentrations in the initially drier soil near the ground surface were below the limit at which nonequilibrium phase change is expected to occur, justifying the use of this more advanced modeling approach. The vapor concentration gradient was greater in the initially wetter soil deeper in the profile
- The initial degree of saturation was observed to influence both heat transfer and water flow in the model with vapor diffusion and phase change, with the greatest change in the degree of saturation occurring for soil with initially higher degrees of saturation.

ACKNOWLEDGMENTS

Funding from National Science Foundation grant CMMI 1230237 is much appreciated. The opinions are those of the authors alone and do not reflect the viewpoint of the sponsor.

REFERENCES

Acuña, J., Fossa, M., Monzó, P., and Palm, B. (2012). "Numerically generated g-functions for ground coupled heat pump applications." Proceedings of the COMSOL Multiphysics Conference, Milan. COMSOL, Brescia. 1-6.

Armstrong, J.E., Frind, E.O. and McClellan, R.D. (1994). "Nonequilibrium mass transfer between the vapor, aqueous, and soil-phases in unsaturated soils during vapor extraction." Water Resour. Res., 30, 355–368.

Baladi, J.Y., Ayers, D.L., and Schoenhals, R.J. (1981). "Transient heat and mass transfer in soils." International Journal of Heat and Mass Transfer. 24(3), 449–458.

Başer, T., Lu, N., and McCartney, J.S. (2016a). "Operational response of a soil-borehole thermal energy storage system." ASCE Journal of Geotechnical and Geoenvironmental Engineering. 142(4), 04015097-1-12. 10.1061/(ASCE)GT.1943-5606.0001432.

Başer, T., Traore, T. and McCartney, J.S. (2016b). "Physical modeling of coupled heat transfer and water flow in soil-borehole thermal energy storage systems in the vadose zone." In: Geothermal Energy: An Emerging Resource. C.B. Dowling, L.J. Florea, and K. Neumann, eds. GSA Books. Boulder, CO. Geological Society of America Special Paper 519. 81-93.

Başer, T., Dong, Y., Lu, N., and McCartney, J.S. (2016c). "Role of considering non-constant soil thermal parameters in the simulation of geothermal heat storage systems in the vadose zone." Proceedings of ISSMGE 8th AYGEC, Astana, Kazakhstan, 1-6.

Bear, J. (1972). Dynamics of Fluids in Porous Media. Dover, Mineola, N.Y., 764.

Beier, R.A., Acuña, J., Mogensen, P., and Palm, B. (2014). "Transient heat transfer in a coaxial borehole heat exchanger." Geothermics. 51, 470-482.

Bénet, J.C., and Jouanna, P. (1982). "Phenomenological relation of phase change of water in a porous-medium-experimental verification and measurement of the phenomenological coefficient." Int. J. Heat Mass Trans. 25, 1747–1754.

Bénet, J.C., Lozano, A.L. Cherblanc, F. and Cousin, B. (2009). "Phase change of water in a hygroscopic porous medium: Phenomenological relation and experimental analysis for water in soil." Journal of Non-Equilibrium Thermodynamics. 34, 133–153.

Bixler, N.E. (1985). NORIA: A Finite Element Computer Program for Analyzing Water, Vapor, Air and Energy Transport in Porous Media. SAND84-2057, Sandia National Laboratories, Albuquerque, NM.

513 Bouyoucos, G.J. (1915). “Effect of temperature on movement of water vapor and capillary
514 moisture in soils.” Journal of Agricultural Research. 4, 141-172.
515 Campbell, G.S. (1985). Soil Physics with BASIC: Transport Models for Soil–Plant Systems.
516 Elsevier, New York.
517 Campbell, G.S., Jungbauer, J.D., Bidlake, W.R., and Hungerford, R.D. (1994). “Predicting the
518 eff ect of temperature on soil thermal conductivity.” Soil Science. 158, 307–313.
519 Cass, A., Campbell, G.S., and Jones. T.L. (1984.) “Enhancement of thermal water vapor diffusion
520 in soil.” Soil Science Society of America. 48(1), 25–32.
521 Catolico, N., Ge, S., and McCartney, J.S. (2016). “Numerical modeling of a soil-borehole thermal
522 energy storage system.” Vadose Zone Journal. 15(1), 1-17. doi:10.2136/vzj2015.05.0078.
523 Chammari, A., Naon, B., Cherblanc, F., Cousin, B., and Bénet, J.C. (2008). “Interpreting the
524 drying kinetics of a soil using a macroscopic thermodynamic nonequilibrium of water between
525 the liquid and vapor phase.” Drying Technology. 26, 836–843.
526 Chapuis, S. and Bernier, M. (2009). “Seasonal storage of solar energy in borehole heat
527 exchangers.” Proc. IBPSA Conf. Building Simulations, Glasgow, Scotland. 599-606.
528 Ciriello, V., Bottarelli, M., Di Federico V., and Tartakovsky, D.M. (2015). “Temperature fields
529 induced by geothermal devices.” Energy. 93(2), 1896-1903.
530 Claesson, J. and Hellström, G. (1981). “Model studies of duct storage systems. New energy
531 conservation technologies and their commercialization.” J.P. Millhone and E.H. Willis, eds.,
532 Springer, Berlin.762–778.
533 Cleall, P.J., Singh, R.M., and Thomas, H.R. (2011). “Non-isothermal moisture movement in
534 unsaturated kaolin: An experimental and theoretical investigation.” Geotechnical Testing
535 Journal. 34(5), 1-11.

536 Cleall, P.J., Seetharam, S.C., Thomas, H.R. (2007). “Inclusion of some aspects of chemical
537 behaviour of unsaturated soil in thermo/hydro/chemical/mechanical models. I: Model
538 development.” ASCE Journal of Engineering Mechanics. 133(3), 338–47.
539 Côté, J. and Konrad, J.-M. (2005). Thermal conductivity of base course materials. Canadian
540 Geotechnical Journal, 42, 61–78.
541 Dong, Y., McCartney, J.S, Lu, N. (2015). “Critical review of thermal conductivity models for
542 unsaturated soils.” Geotechnical and Geological Engineering. 33(2), 207-221.
543 Eskilson, P. (1987). Thermal Analysis of Heat Extraction Boreholes. Dept. of Mathematical
544 Physics, Lund Univ. Lund, Sweden.
545 Ewen, J. (1988). “Thermal instability in gently heated unsaturated sand.” International Journal of
546 Heat and Mass Transfer. 31(8), 1707-1710.
547 Ewen, J. and Thomas, H.R. (1989). “Heating unsaturated medium sand.” Géotechnique. 39(3),
548 455-470.
549 Farouki, O.T. (1981). Thermal Properties of Soils. Cold Regions Science and Engineering,
550 CRREL, Monograph 81-1, 136.
551 Gehlin, S. (2002). Thermal Response Test: Method Development and Evaluation. Doctoral Thesis.
552 Lulea University of Technology.
553 Gens, A., Garcia Molina, A., Olivella, S., Alonso, E.E., Huertas, F. (1998). “Analysis of a full
554 scale in-situ test simulating repository conditions.” International Journal for Numerical and
555 Analytical Methods in Geomechanics. 22(7), 515–48.
556 Gens, A., Vaunat, J., Garitte, B., Wileveau, Y. (2007). “In situ behaviour of a stiff layered clay
557 subject to thermal loading: observations and interpretation.” Géotechnique. 57(2), 207–28.

558 Gens, A., Sánchez, M., Guimarães, L.M., Alonso, E.E., Lloret, A., Olivella, S., Villar, M.V., and
559 Huertas, F. (2009). "A full scale in situ heating test for high level nuclear waste disposal:
560 observations, analysis and interpretation." Géotechnique. 59(4), 377–99.
561 Grant, S.A. and Salehzadeh, A. (1996). "Calculations of temperature effects on wetting
562 coefficients of porous solids and their capillary pressure functions." Water Resources Res.
563 32(2), 261–279.
564 Guimarães, L.M., Gens, A., Olivella, S. (2007). "Coupled thermo-hydro-mechanical and chemical
565 analysis of expansive clay subjected to heating and hydration." Transport in Porous Media.
566 66(3), 341–72.
567 Guimarães, L., Gens, A., Sánchez, M., Olivella, S. (2013). "A chemo-mechanical constitutive
568 model accounting for cation exchange in expansive clays." Géotechnique. 63(3), 221–34.
569 Gurr, C.G., Marshall, T.J., and Hutton, J.T. (1952). "Movement of water in soil due to a
570 temperature gradient." Soil Science. 74(5), 335-345.
571 Hillel, D. (1980). Fundamental of Soil Physics. Academic, San Diego, CA.
572 Ingersoll, L.R. and Plass, H.J. (1948). "Theory of the ground pipe heat source for the heat pump."
573 Heating, Piping and Air Conditioning. 20(7), 119-122
574 Ingersoll, L.R., Zobel, O.J., and Ingersoll, A.C. (1954). Heat Conduction with Engineering,
575 Geological, and Other Applications. University of Wisconsin Press. Revised edition, 325.
576 Kavanaugh, S.P. (1998). "A design method for hybrid ground-source heat pumps." ASHRAE
577 Transactions. 104(2), 691-698.
578 Lamarche, L. and Beauchamp, B. (2007). "A new contribution to the finite line-source model for
579 geothermal boreholes. Energy and Buildings. 39(2), 188-198.
580 Lide, D.R. (Ed.) (2001). Handbook of Chemistry and Physics, CRC Press, Boca Raton, FL.

581 Lozano, A.-L., Cherblanc, F., Cousin, B., and Benet, J.-C. (2008). "Experimental study and
582 modelling of the water phase change kinetics in soils." European Journal of Soil Science. 59(5),
583 939-949.
584 Lu, N. and Dong, Y. (2015). "A closed form equation for thermal conductivity of unsaturated soils
585 at room temperature." Journal of Geotech. and Geoenv. Eng. 141(6), 04015016.
586 McCartney, J.S., Ge, S., Reed, A., Lu, N., and Smits, K. (2013). "Soil-borehole thermal energy
587 storage systems for district heating." Proc., European Geothermal Congress 2013, European
588 Geothermal Energy Council, Brussels, Belgium. 1-10.
589 McCartney, J.S., Başer, T., Zhan, N., Lu, N., Ge, S., and Smits, K. (2017). "Storage of solar
590 thermal energy in borehole thermal energy storage systems." IGSHPA Technical Conference
591 and Expo. Denver, CO. Mar. 14-17. 1-8.
592 Millington, R.J., and Quirk, J.M. (1961). "Permeability of porous solids." Trans. Faraday Soc. 57,
593 1200–1207.
594 Monteith, J.L. and Unsworth, M.H. (1990). Principles of Environmental Physics. Routledge
595 Chapman and Hall, New York, NY.
596 Moradi, A.M., Smits, K., Massey, J., Cihan, A., and McCartney, J.S. (2015). "Impact of coupled
597 heat transfer and water flow on soil borehole thermal energy storage (SBTES) systems:
598 Experimental and modeling investigation." Geothermics. 57(September), 56-72.
599 Moradi, A.M., Smits, K., Lu, N., and McCartney, J.S. (2016). "3-D experimental and numerical
600 investigation of heat transfer in unsaturated soil with an application to soil borehole thermal
601 energy storage (SBTES) systems." Vadose Zone J. 15(10), 1-17.
602 Nordell, B. and Hellström, G. (2000). "High temperature solar heated seasonal storage system for
603 low temperature heating of buildings." Applied Energy. 69(6), 511–523.

604 Olivella, S., Gens, A., Carrera, J., Alonso, E.E. (1996). “Numerical formulation for a simulator
605 (CODE-BRIGHT) for the coupled analysis of saline media.” Engineering with Computers.
606 3(7), 87–112.
607 Ozudogru, T.Y., Ghasemi-Fare, O., Olgun, C.G, and Basu P. (2015). “Numerical modeling of
608 vertical geothermal heat exchangers using finite difference and finite element techniques.”
609 Geotechnical and Geological Engineering. 33, 291-306. doi:10.1007/s10706-014-9822-z.
610 Penman, H.L. (1940). “Gas and vapor movement in soil: I. The diffusion of vapors in porous
611 solids.” J. Agric. Sci. 30, 437–462.
612 Philip, J.R., and de Vries, D.A. (1957). “Moisture movement in porous materials under
613 temperature gradients.” Trans. Amer. Geophys. Union 38(2), 222–232.
614 Richards, L.A. (1931). “Capillary conduction of liquids through porous mediums.” Physics. 1(5):
615 318–333
616 Saito, H., Simunek, J., Mohanty, B.P. (2006). “Numerical analysis of coupled water, vapor, and
617 heat transport in the vadose zone.” Vadose Zone Journal. 5, 784-800.
618 Shah, D.J., Ramsey, J.W., and Wang, M. (1984). “An experimental determination of the heat and
619 mass transfer coefficients in moist, unsaturated soils.” International Journal of Heat and Mass
620 Transfer, 27(7), 1075–1085.
621 Sibbitt, B., McClenahan, D., Djebbar, R., Thornton, J., Wong, B., Carriere, J., Kokko, J. (2012).
622 “The performance of a high solar fraction seasonal storage district heating system - Five years
623 of operation.” Energy Procedia. 30, 856-865.
624 Smith, W.O. (1943). “Thermal transfer of moisture in soils.” Am. Geophys. Union Trans. 24 (2),
625 511–524.

626 Smits, K.M., Cihan, A., Sakaki, S., and Illangasekare, T.H. (2011). "Evaporation from soils under
627 thermal boundary conditions: Experimental and modeling investigation to compare
628 equilibrium- and nonequilibrium-based approaches." Water Resources Research. 47, W05540,
629 doi:10.1029/2010WR009533.
630 Smits, K.M., Sakaki, S., Howington, S.E., Peters, J.F., and Illangasekare, T.H. (2013).
631 "Temperature dependence of thermal properties of sands across a wide range of temperatures
632 (30-70 °C)." Vadose Zone Journal. doi: 10.2136/vzj2012.0033.
633 Tarn, J.Q. and Wang, Y.M. (2004). "End effects of heat conduction in circular cylinders of
634 functionally graded materials and laminated composites." International Journal of Heat and
635 Mass Transfer. 47, 5741–5747.
636 Thomas, H.R. and He, Y. (1997). "A coupled heat-moisture transfer theory for deformable
637 unsaturated soil and its algorithmic implementation." International Journal of Numerical
638 Methods in Engineering. 40, 3421-3441.
639 Thomas, H.R. and King, S.D. (1991). "Coupled temperature capillary potential variations in
640 unsaturated soil." Journal of Engineering Mechanics. ASCE. 117(11), 2475-2491.
641 Thomas, H.R. and Sansom, M.R. (1995). "Fully coupled analysis of heat, moisture and air transfer
642 in unsaturated soil." Journal of Engineering Mechanics. 121(3), 392-405.
643 Thomas, H.R., He, Y., Sansom, M.R., Li, C.L.W. (1996). "On the development of a model of the
644 thermo-mechanical-hydraulic behavior of unsaturated soils." Engineering Geology. 41, 197-
645 218.
646 Thomas, H.R., Sansom, M., and Rees, S.W. (2001). "Non-isothermal flow." In: Environmental
647 Geomechanics. Springer. 131-169.

Trautz, A.C., Smits, K.M., and Cihan, A. (2015). "Continuum-scale investigation of evaporation from bare soil under different boundary and initial conditions: An evaluation of nonequilibrium phase change." Water Resources Research. 51, 7630–7648.

van Genuchten, M.T. (1980). "A closed-form equation for predicting the hydraulic conductivity of unsaturated soils." Soil Sci. Soc. Am. J. 44(5), 892–898.

Wayllace, A. and Lu, N. (2012) "A transient water release and imbibitions method for rapidly measuring wetting and drying soil water retention and hydraulic conductivity functions." Geotechnical Testing Journal 35(1), 103-117.

Whitaker, S. (1977). "Simultaneous heat, mass and momentum transfer in porous media: A theory of drying porous media." Adv. Heat Transf. 13, 119–203.

Welsch, B., Rühaak, W., Schulte, D.O., Bär, K., Homuth, S., and Sass, I. (2015). "Comparative study of medium deep borehole thermal energy storage systems using numerical modelling." Proc. World Geothermal Congress 2015. International Geothermal Association. Bochum. 1-6.

Zhang, J. and Datta, A.K. (2004). "Some considerations in modeling of moisture transport in heating of hygroscopic materials." Drying Technology. 22(8), 1983-2008.

665 **TABLE 1.** Equations used in the numerical analyses

Equation	Number	Reference
Nonisothermal liquid flow governing equation: $$nS_{rw}\frac{\partial \rho_w}{\partial t}+n\rho_w\frac{dS_{rw}}{dP_c}\frac{\partial P_c}{\partial t}+\nabla\cdot\left[\rho_w\left(-\frac{k_{rw}\kappa}{\mu_w}\right)\nabla\left(P_w+\rho_w gz\right)\right]=-R_{gw}$$ n=porosity (m^3/m^3), S_{rw}=degree of water saturation (m^3/m^3), ρ_w=temperature-dependent density of water (kg/m^3) (Hillel 1980), t=time(s), $P_c=P_w-P_g$=capillary pressure (Pa), P_w=pore water pressure (Pa), P_g=pore gas pressure (Pa), k_{rw}=relative permeability function for water (m/s); κ=intrinsic permeability (m^2); μ_w=temperature-dependent water dynamic viscosity (kg/(ms)) (Lide 2001), g=acceleration due to gravity (m/s^2) R_{gw}=Phase change rate (kg/m^3s)	(1)	(Bear 1972; Moradi et al. 2016)
Nonisothermal gas flow governing equation: $$nS_{rg}\frac{\partial \rho_g}{\partial t}+n\rho_g\frac{dS_{rg}}{dP_c}\frac{\partial P_c}{\partial t}+\nabla\cdot\left[\rho_g\left(-\frac{k_{rg}\kappa}{\mu_g}\right)\nabla\left(P_g+\rho_g gz\right)\right]=R_{gw}$$ S_{rg}=degree of gas saturation (m^3/m^3), ρ_g=temperature-dependent density of gas (kg/m^3) (Smits et al. 2011), k_{rg}=relative permeability function for gas (m/s); μ_g=temperature-dependent gas dynamic viscosity (kg/(ms))	(2)	(Bear 1972; Moradi et al. 2016)
Water vapor mass balance equation: $$n\frac{\partial\left(\rho_g S_{rg} w_v\right)}{\partial t}+\nabla\cdot\left(\rho_g u_g w_v-D_e\rho_g\nabla w_v\right)=R_{gw}$$ $D_e=D_v\tau$=effective diffusion coefficient (m^2/s), D_v=diffusion coefficient of water vapor in air (m^2/s) (Campbell 1985), w_v=mass fraction of water vapor in the gas phase (kg/kg), $\tau=n^{1/3}S_{rg}^{7/3}\eta$=tortuosity (Millington and Quirk 1961)	(3)	(Smits et al. 2011)
Enhancement factor for vapor diffusion, η: $$\eta=a+3S_{rw}-(a-1)\exp\left\{-\left[\left(1+\frac{2.6}{\sqrt{f_c}}\right)S_{rw}\right]^3\right\}$$ a=empirical fitting parameter, f_c= clay content	(4)	(Cass et al. 1984)
Nonequilibrium gas phase change rate, R_{gw} (kg/m^3s): $$R_{gw}=\left(\frac{bS_{rw}RT}{M_w}\right)\left(\rho_{veq}-\rho_v\right)$$ b=empirical fitting parameter (s/m^2), R=universal gas constant (J/molK), $\rho_{veq}=c_{v,sat}R_{h,eq}$=equilibrium vapor density (kg/m^3), T=Temperature (K), $\rho_v=\rho_g w_v$=vapor density (kg/m^3), M_w=molecular weight of water (kg/mol)	(5)	(Bixler 1985; Zhang and Datta 2004; Moradi et al. 2016)
Heat transfer energy balance: $$\left(\rho C_p\right)\frac{\partial T}{\partial t}+\nabla.\left(\left(\rho_w C_{pw}\right)u_w T+\left(\rho_g C_{pg}\right)u_g T-\left(\lambda\nabla T\right)\right)=-L_w R_{gw}+Q$$ ρ=total density of soil (kg/m^3), C_p=specific heat of soil (J/kgK), C_{pw}=specific heat capacity of water (J/kgK), C_{pg}=specific heat capacity of gas (J/kgK), λ=thermal conductivity (W/mK), L_w=latent heat of water vaporization (J/kg), u_w=water velocity (m/s), u_g=gas velocity (m/s), Q=heat source term (W/m^3)	(6)	(Whitaker 1977; Moradi et al. 2016)

LIST OF FIGURE CAPTIONS

FIG. 1. Hydraulic and thermal constitutive relationships and relevant parameters for Bonny silt: (a) SWRC and HCF; (b) TCF and VHCF

FIG. 2. Cross-sectional elevation view of the experimental setup for model calibration with dielectric sensor locations

FIG. 3. Predicted and measured time series from the tank-scale heating test: (a) Soil temperatures for different values of *a*; (b) Changes in degree of saturation for different values of *a*; (c) Soil temperatures for different values of *b*; (d) Changes in degree of saturation for different values of *b*

FIG. 4. Simulated and observed temperatures and changes in degree of saturation: (a) Horizontal temperature profile; (b) Horizontal change in degree of saturation profile; (c) Vertical temperature profile; (d) Vertical change in degree of saturation profile

FIG. 5. Initial and boundary conditions on the quarter domain model for a field-scale geothermal heat exchanger: (a) Thermal; (b) Hydraulic

FIG. 6. Comparisons of the effects of heat transfer mechanisms and heat flux for a 90-day heat injection period followed by cooling: (a) Temperature time series; (b) Degree of saturation time series

FIG. 7. Effects of including vapor flow in the coupled analysis; (a) Radial profiles of temperature at a depth of 9.5 m (an initial degree of saturation of 0.25) at the end of heating and cooling; (b) Radial profiles of degree of saturation profiles before and after heating

FIG. 8. Vertical profiles for comparison of different heat transfer mechanisms: (a) Temperature at the end of a 90-day heat injection period; (b) Degree of saturation at the end of a 90-day

heat injection period; (c) Temperature at the end of a 90-day cooling period; (d) Degree of saturation at the end of a 90-day cooling period

FIG. 9. Effect of initial degree of saturation: (a) Time series of temperature; (b) Time series of degree of saturation; (c) Radial temperature profiles; (d) Radial degree of saturation profiles

FIG. 10. Thermal property evaluation at the end of heat injection: (a) Thermal conductivity profiles; (b) Volumetric heat capacity profiles

FIG. 11. Liquid water flow evaluation: (a) Horizontal profiles of suction at different times; (b) Horizontal profiles of hydraulic conductivity at different times

FIG. 12. Vapor concentrations normalized by the equilibrium vapor concentration: (a) Time series; (b) Horizontal profiles at the end of heating; (c) Vertical profiles at the end of heating

FIG. 13. (a) Distributions of latent heat transfer rate at depths corresponding to initial degrees of saturation of 0.25 and 0.50; (b) Comparison of the total heat injected with the energy due to phase change

Figure 1

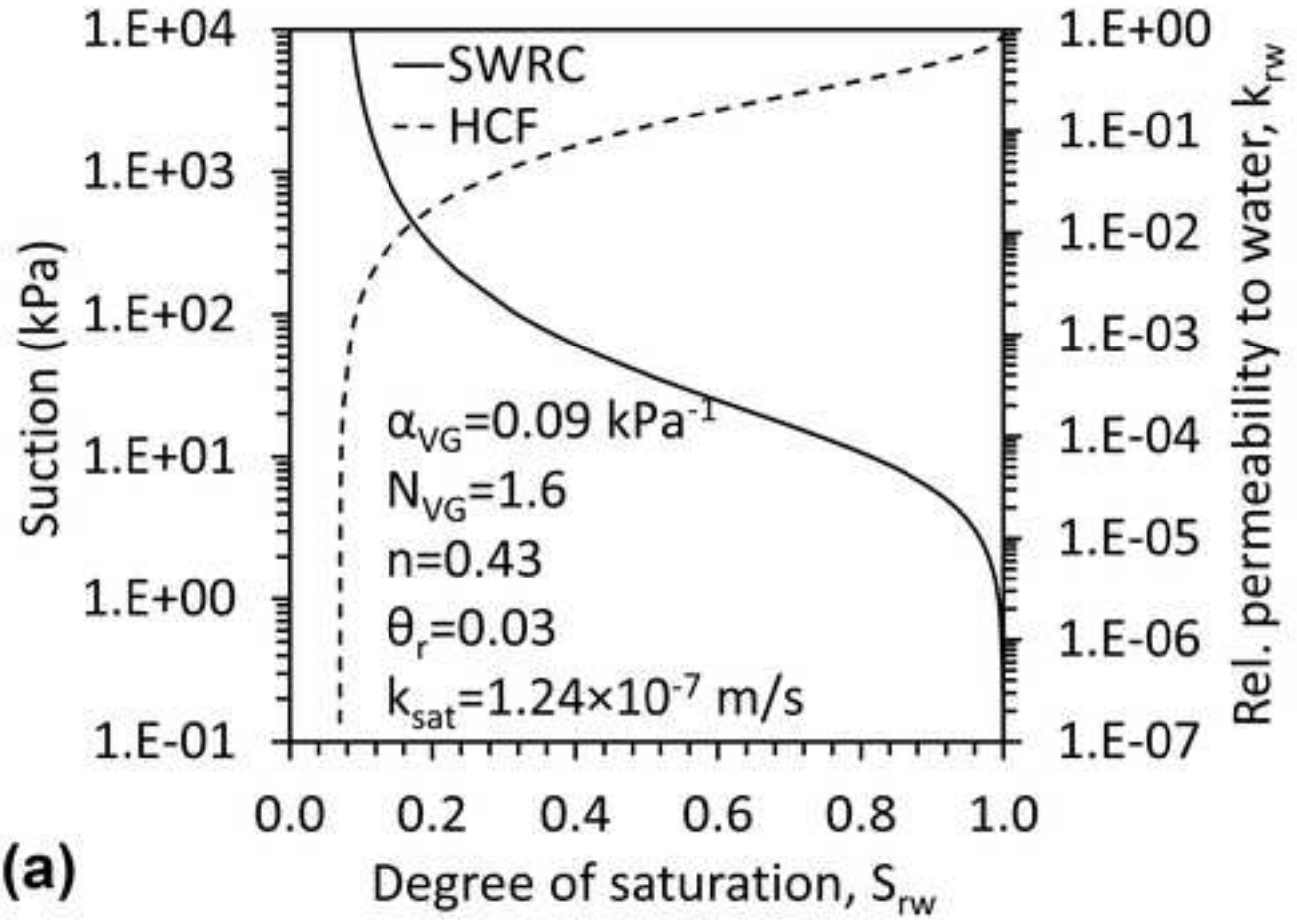

(a)

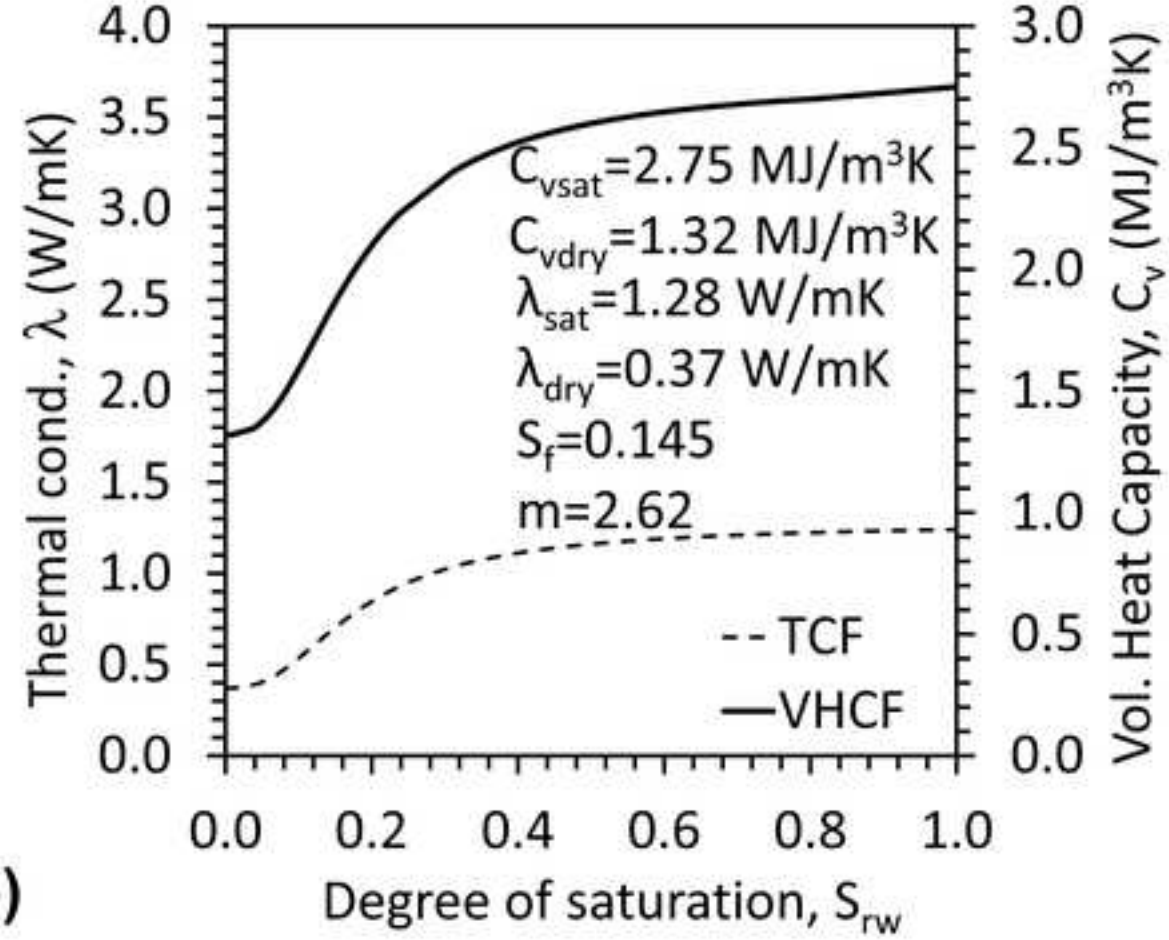

(b)

Figure 2

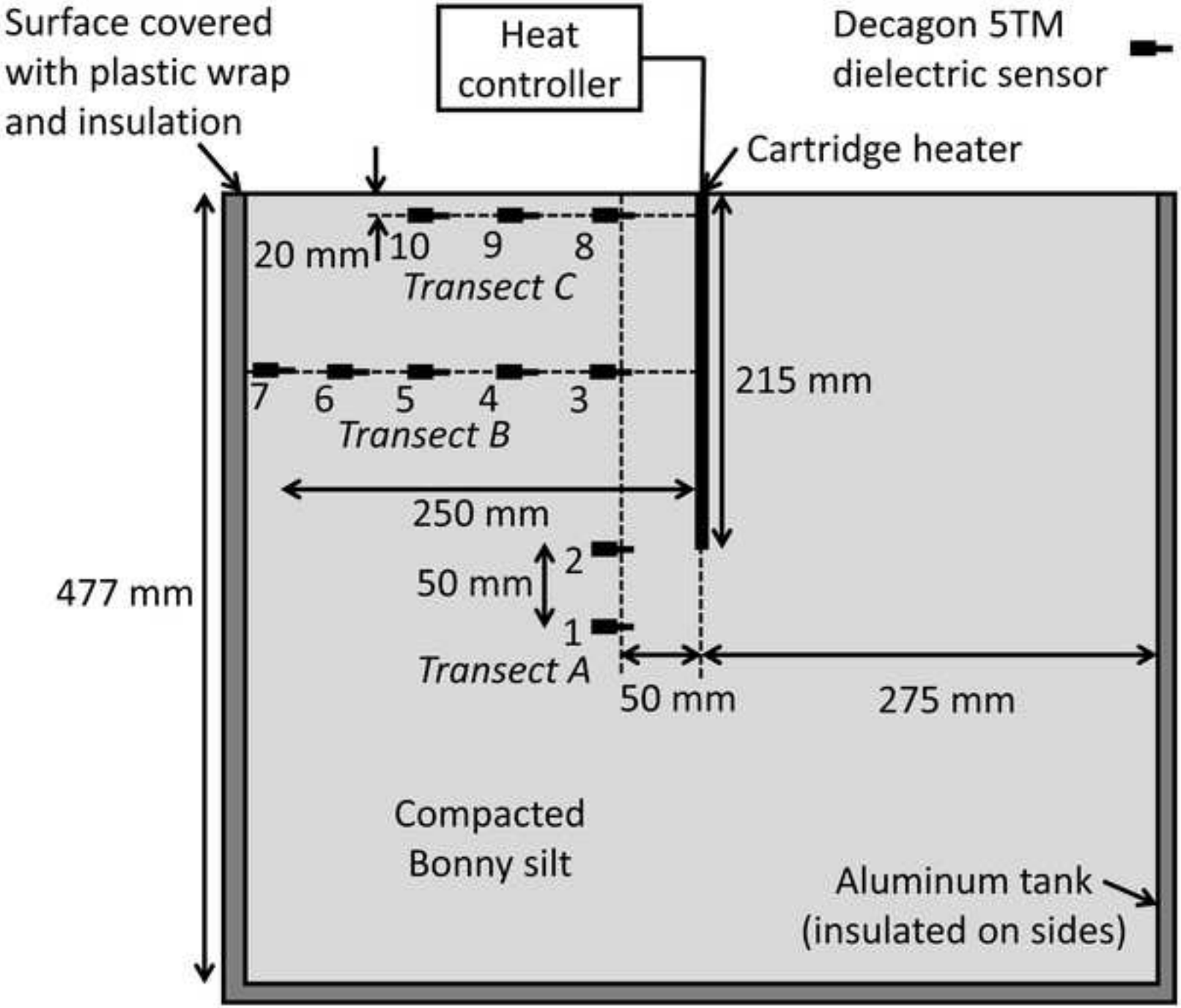

Figure 3

Click here to download Figure Figure 03.tif

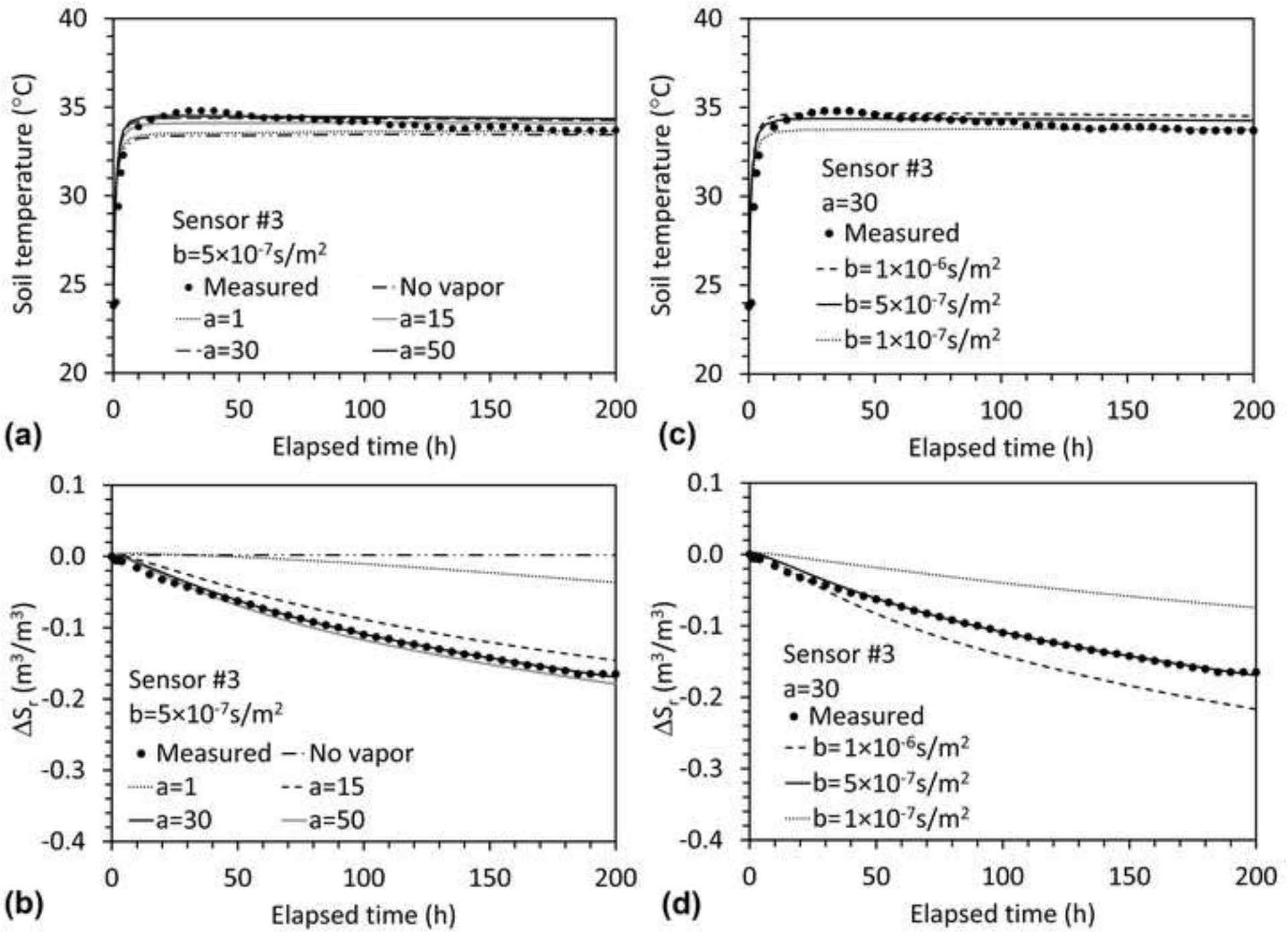

Figure 4

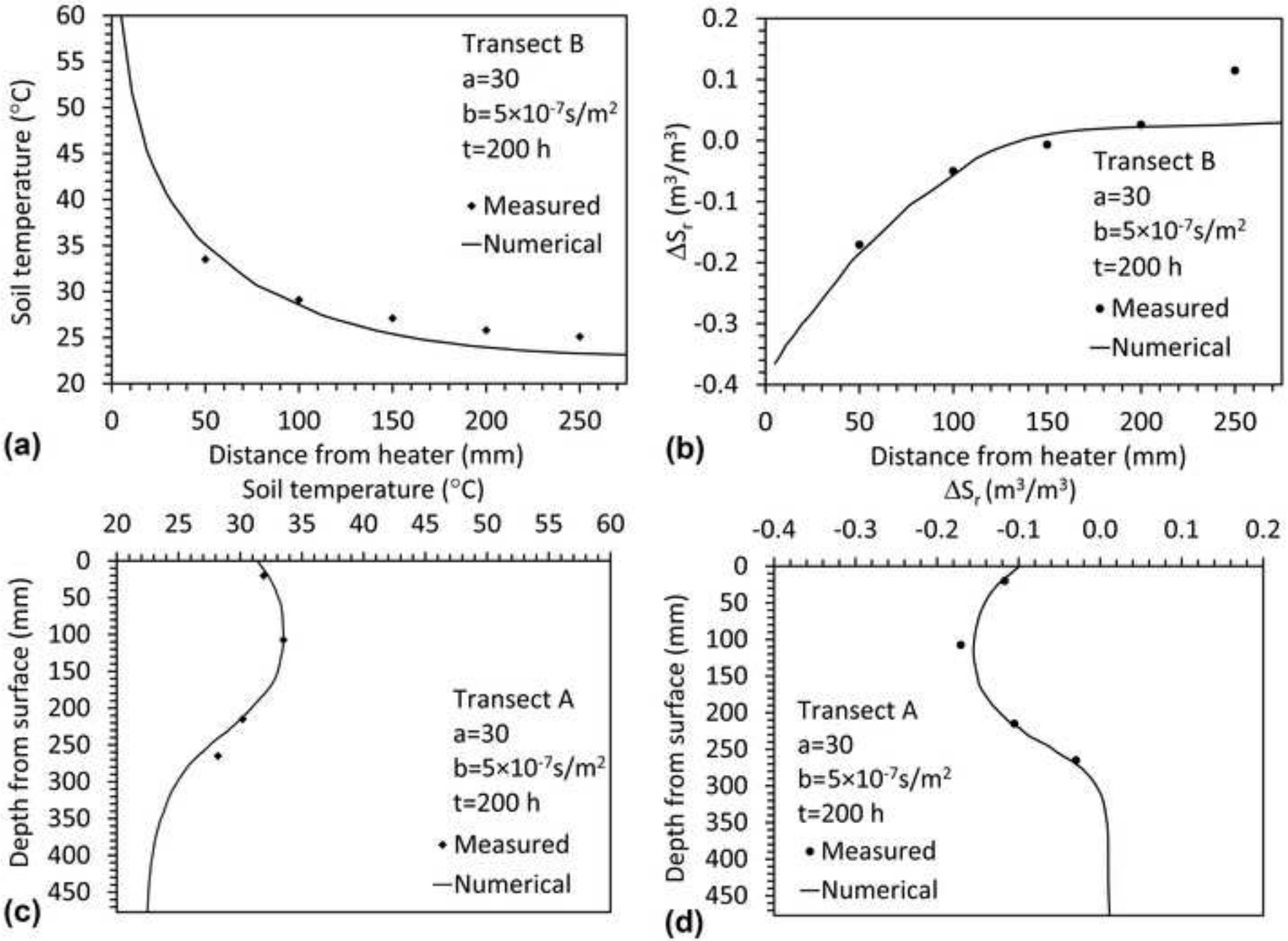

Figure 5

Click here to download Figure Figure 05.tif

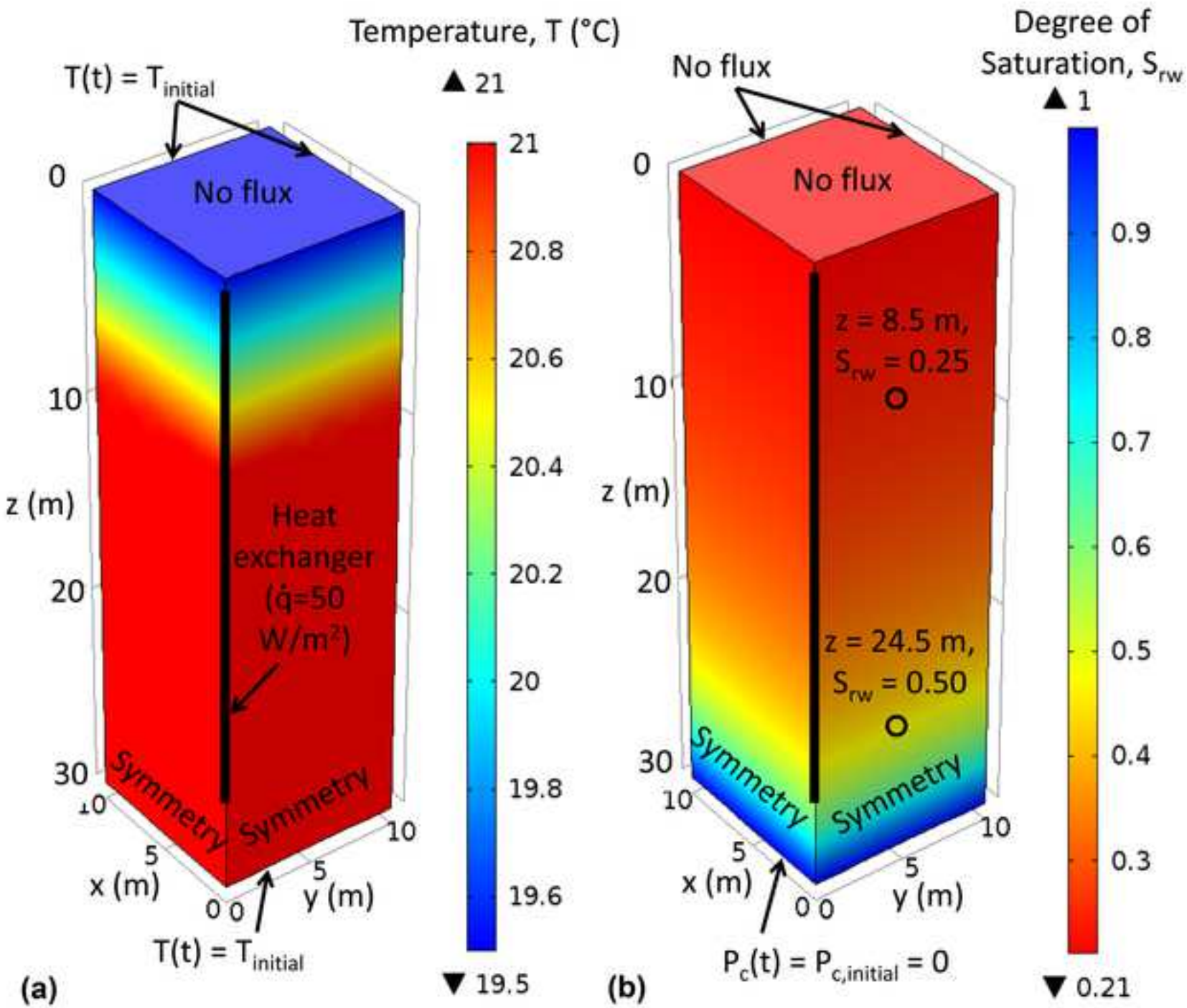

Figure 6

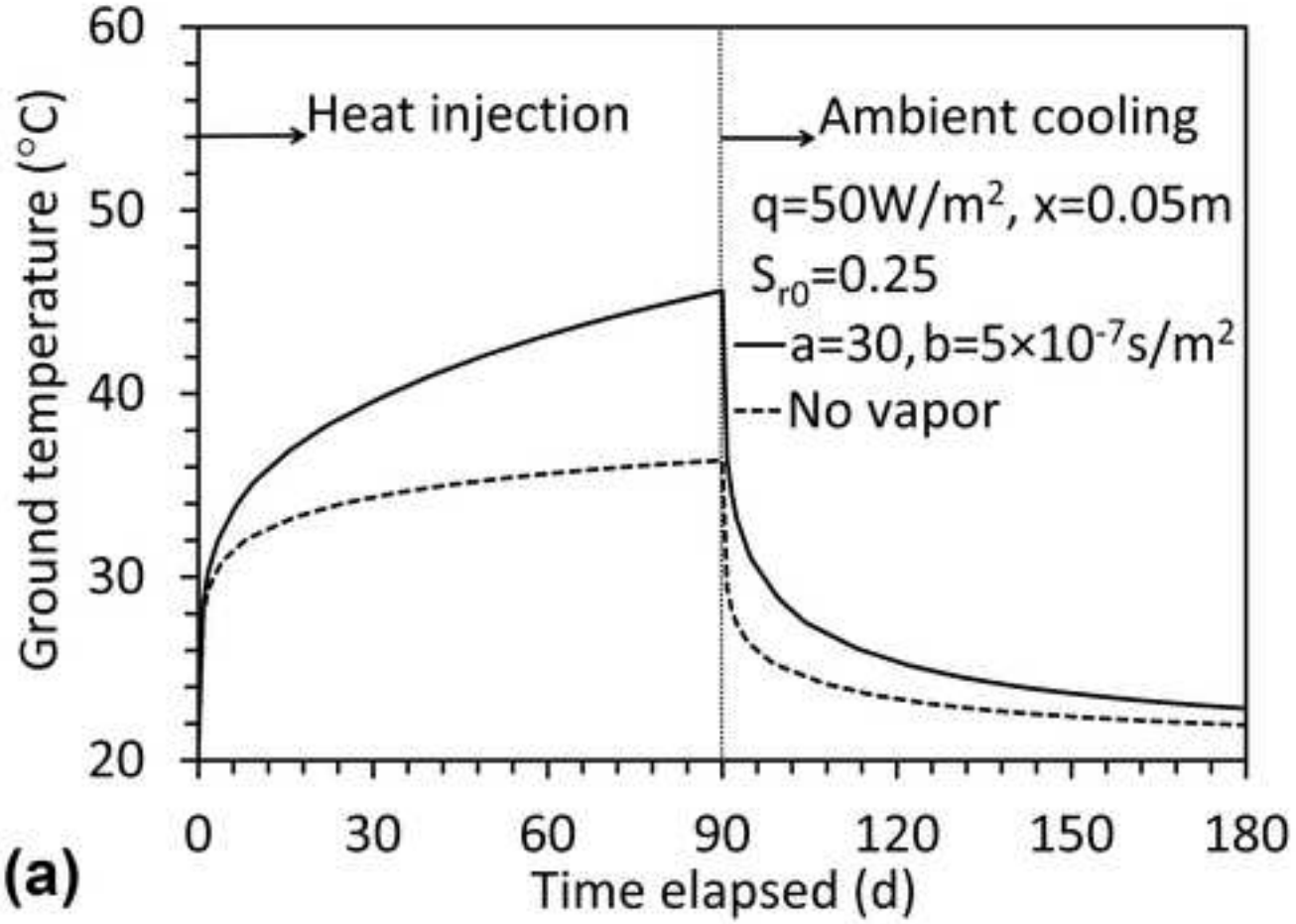

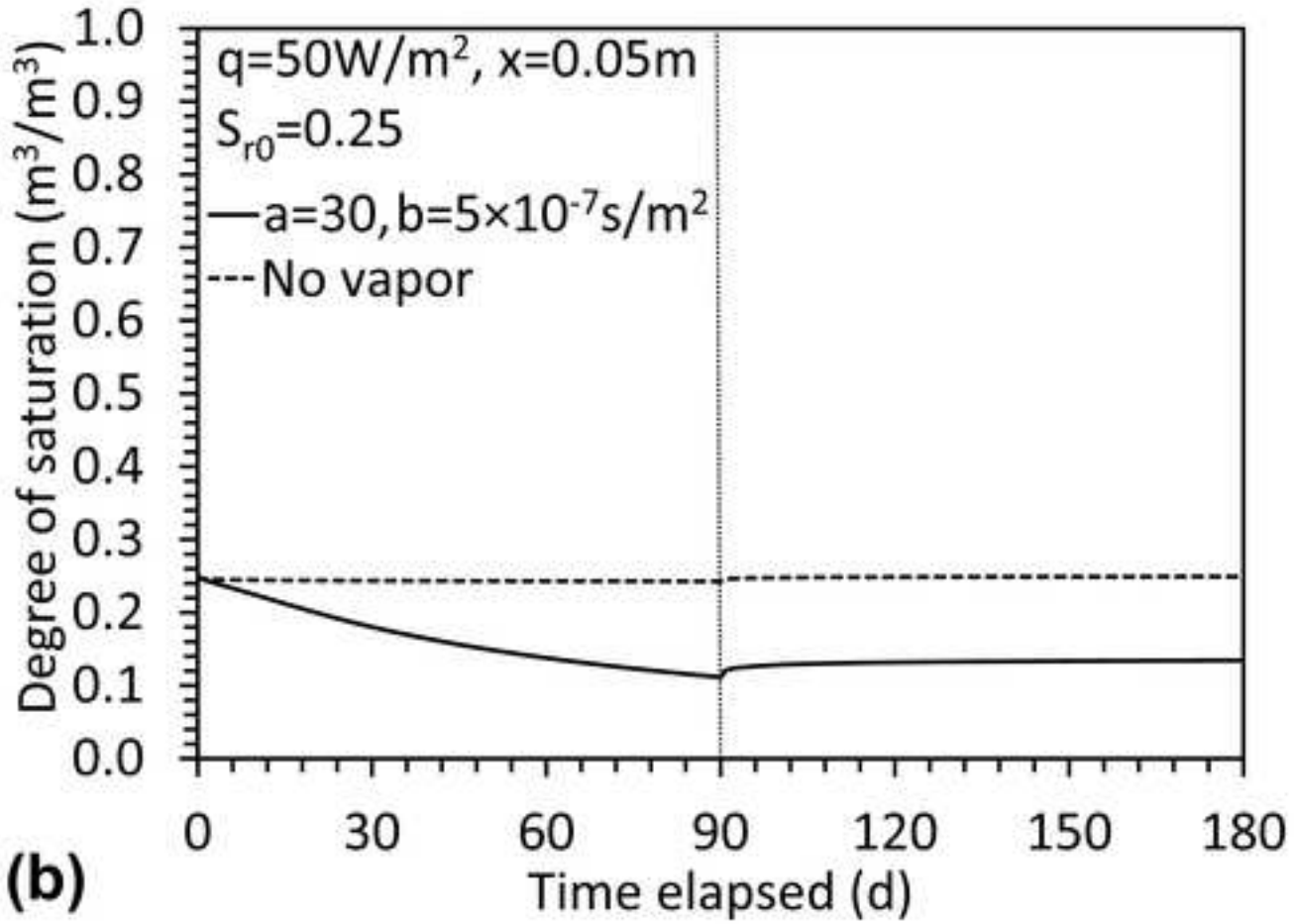

Figure 7

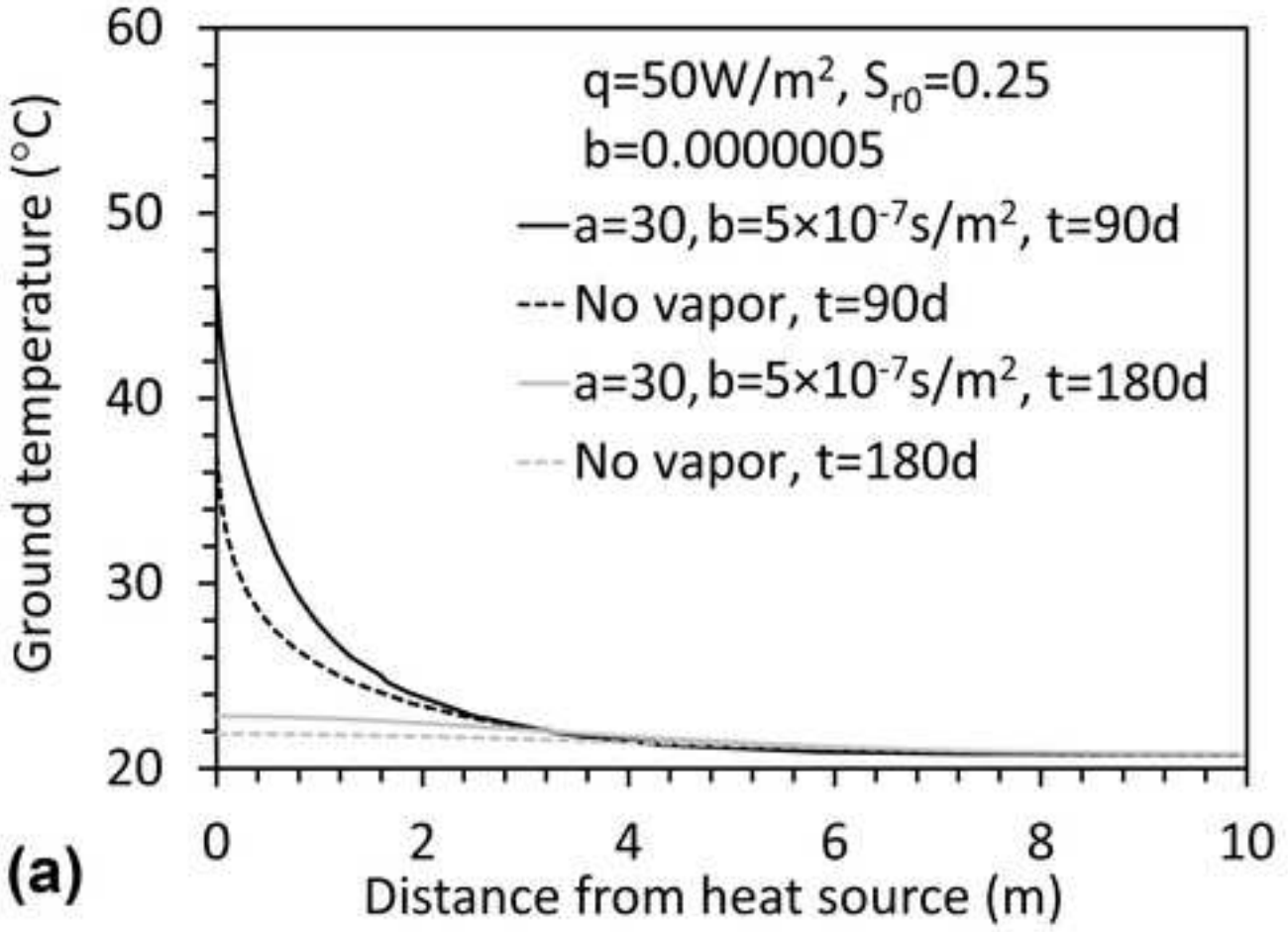

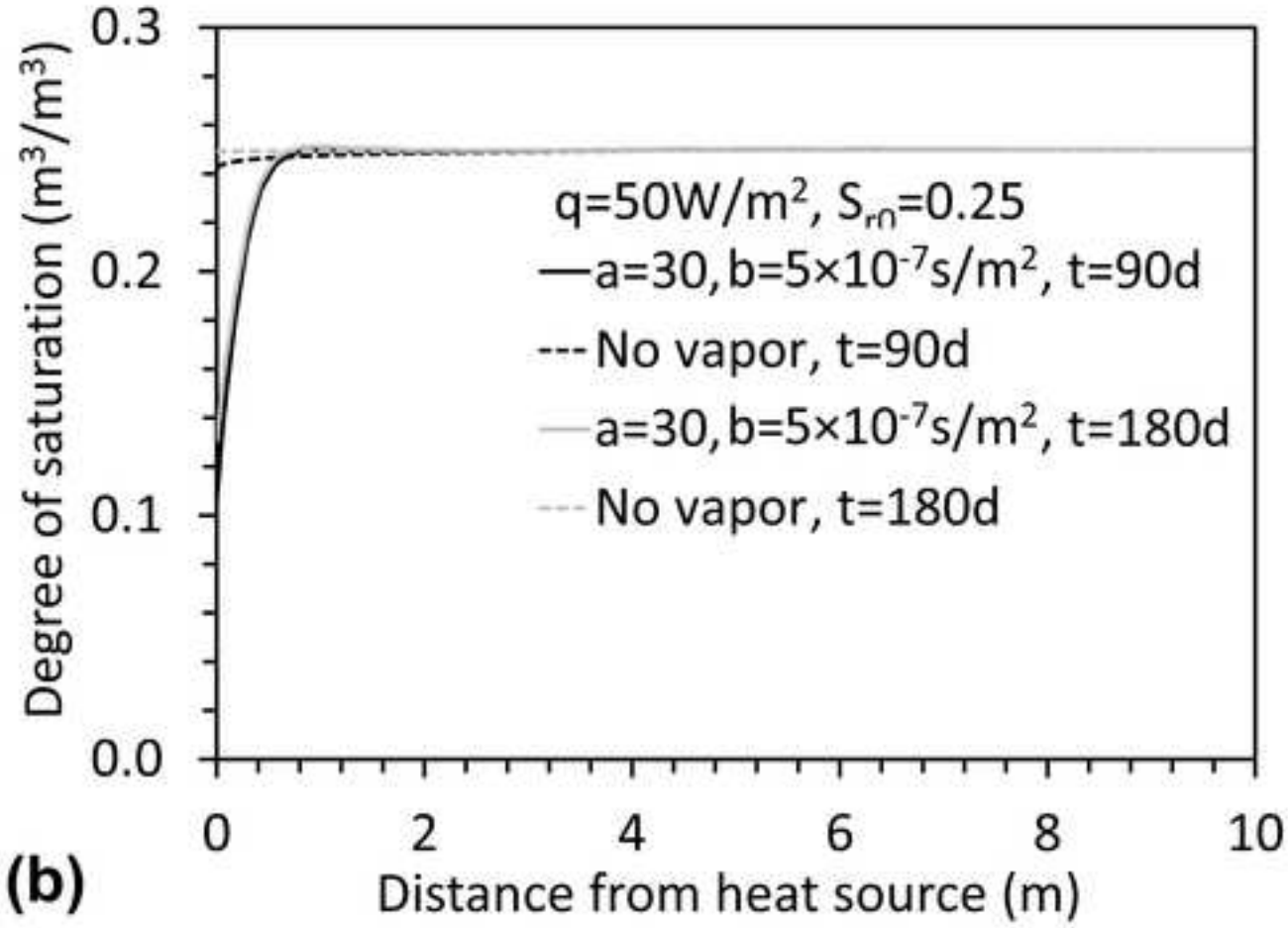

Figure 8

Click here to download Figure Figure 08.tif

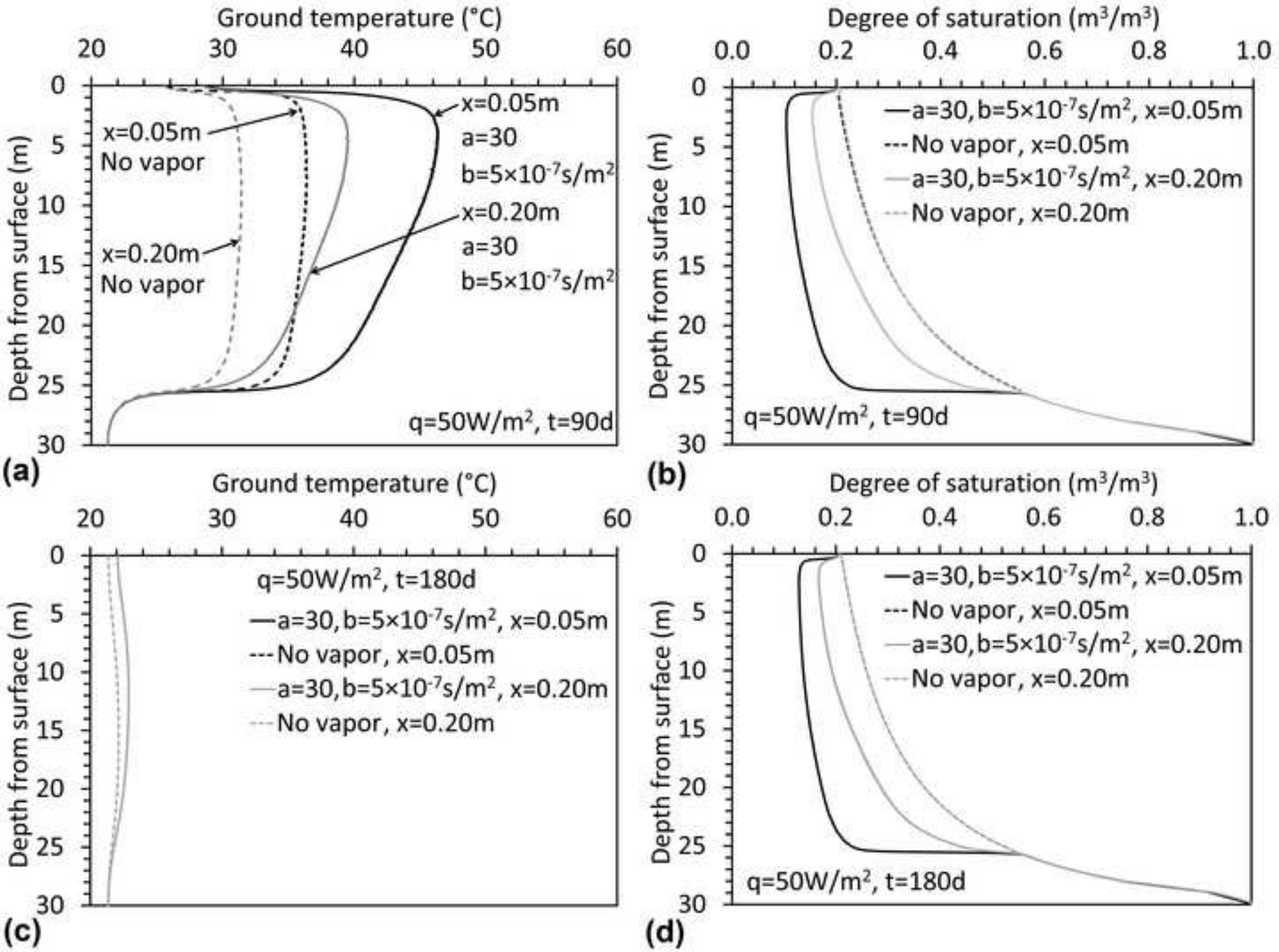

Figure 9

Click here to download Figure Figure 09.tif

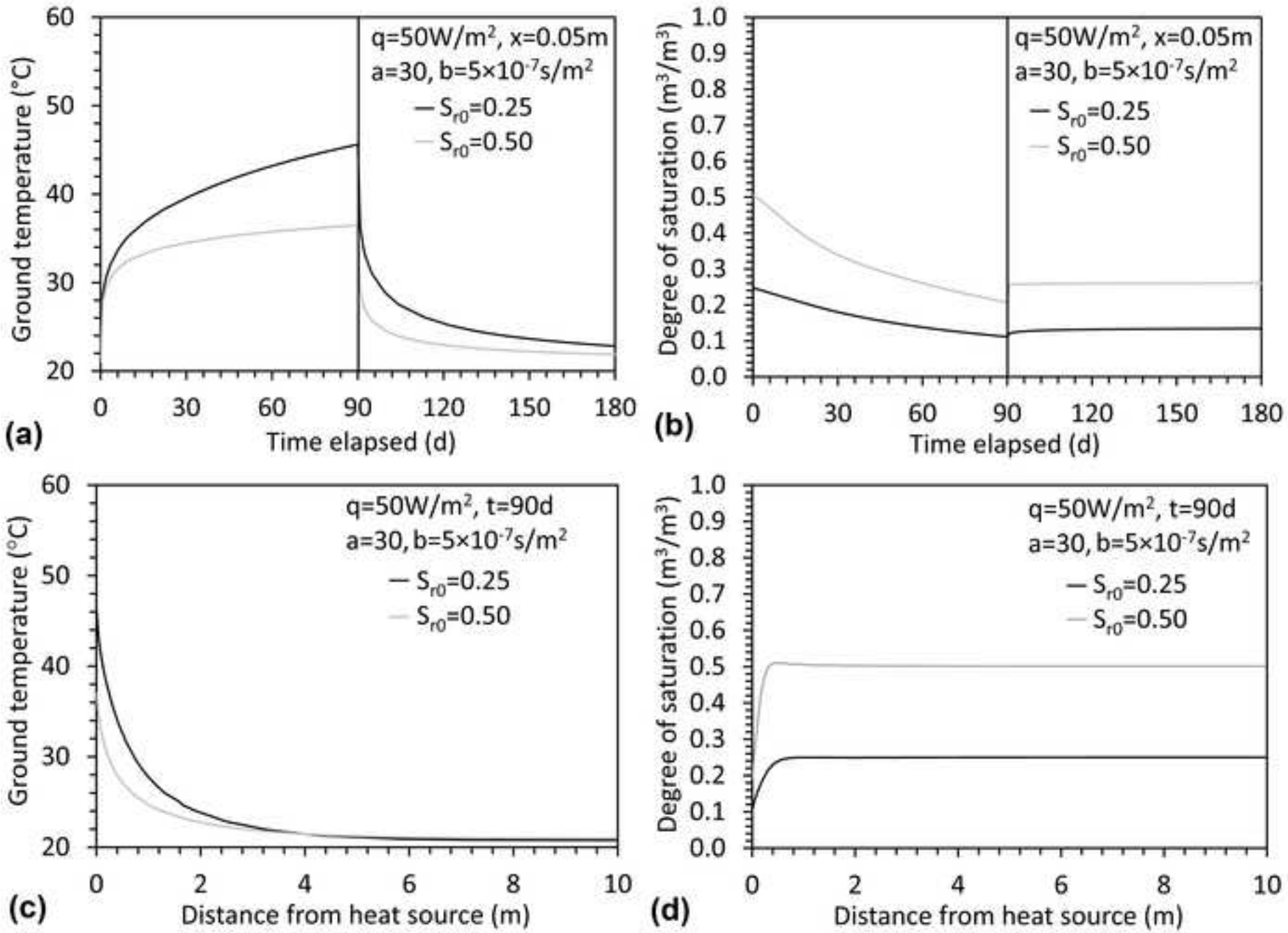

Figure 10

Click here to download Figure Figure 10.tif

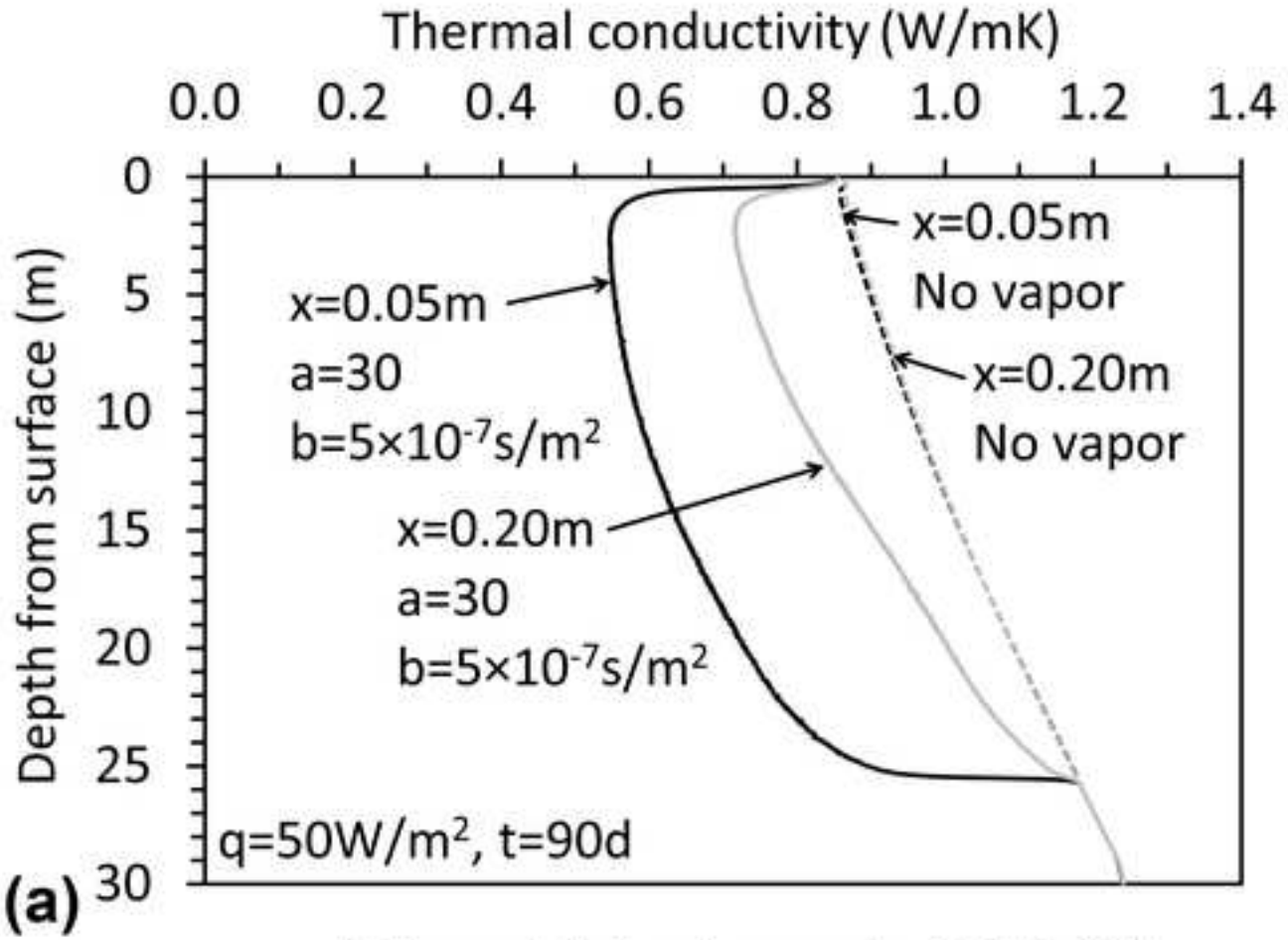

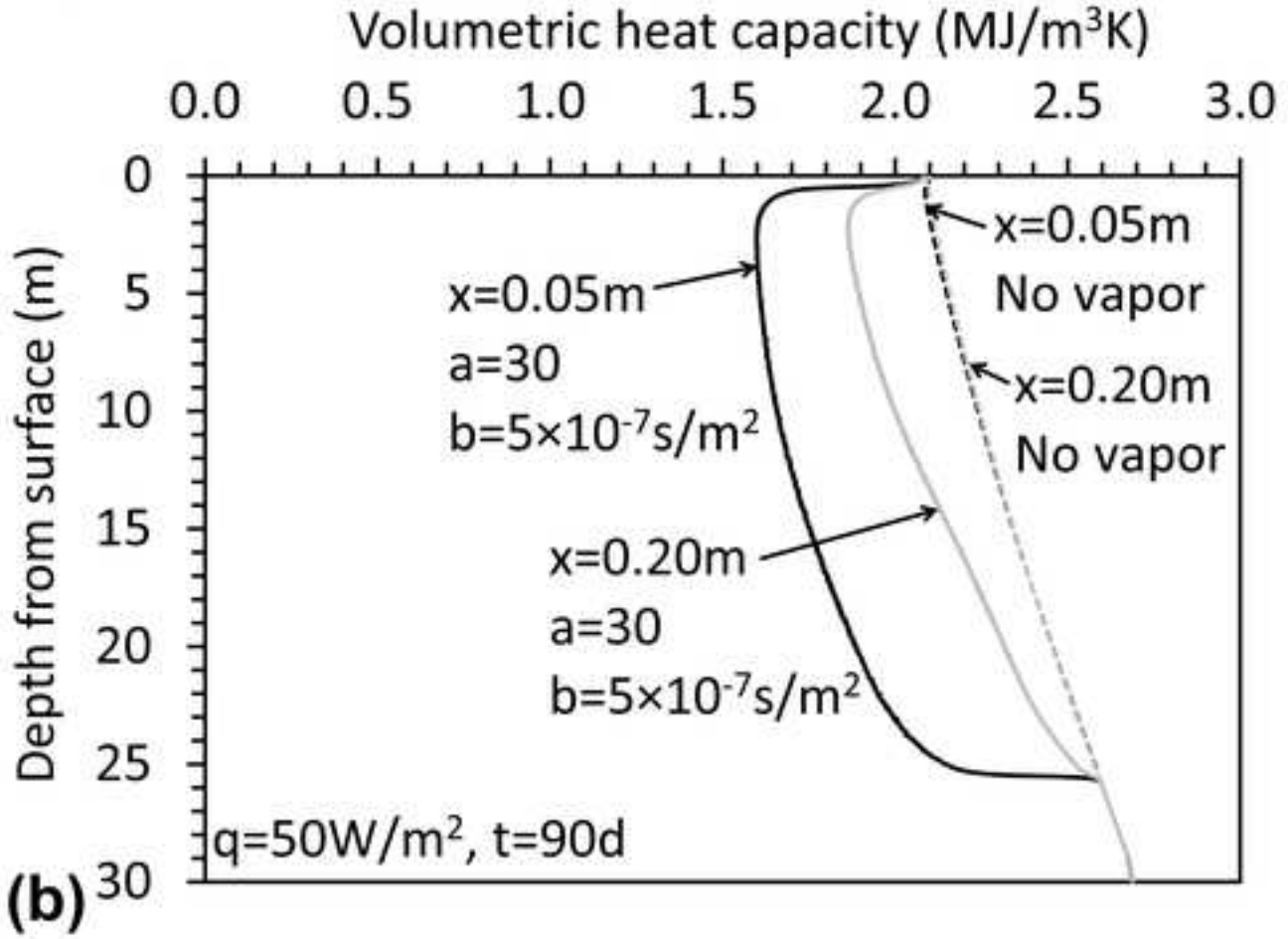

Figure 11

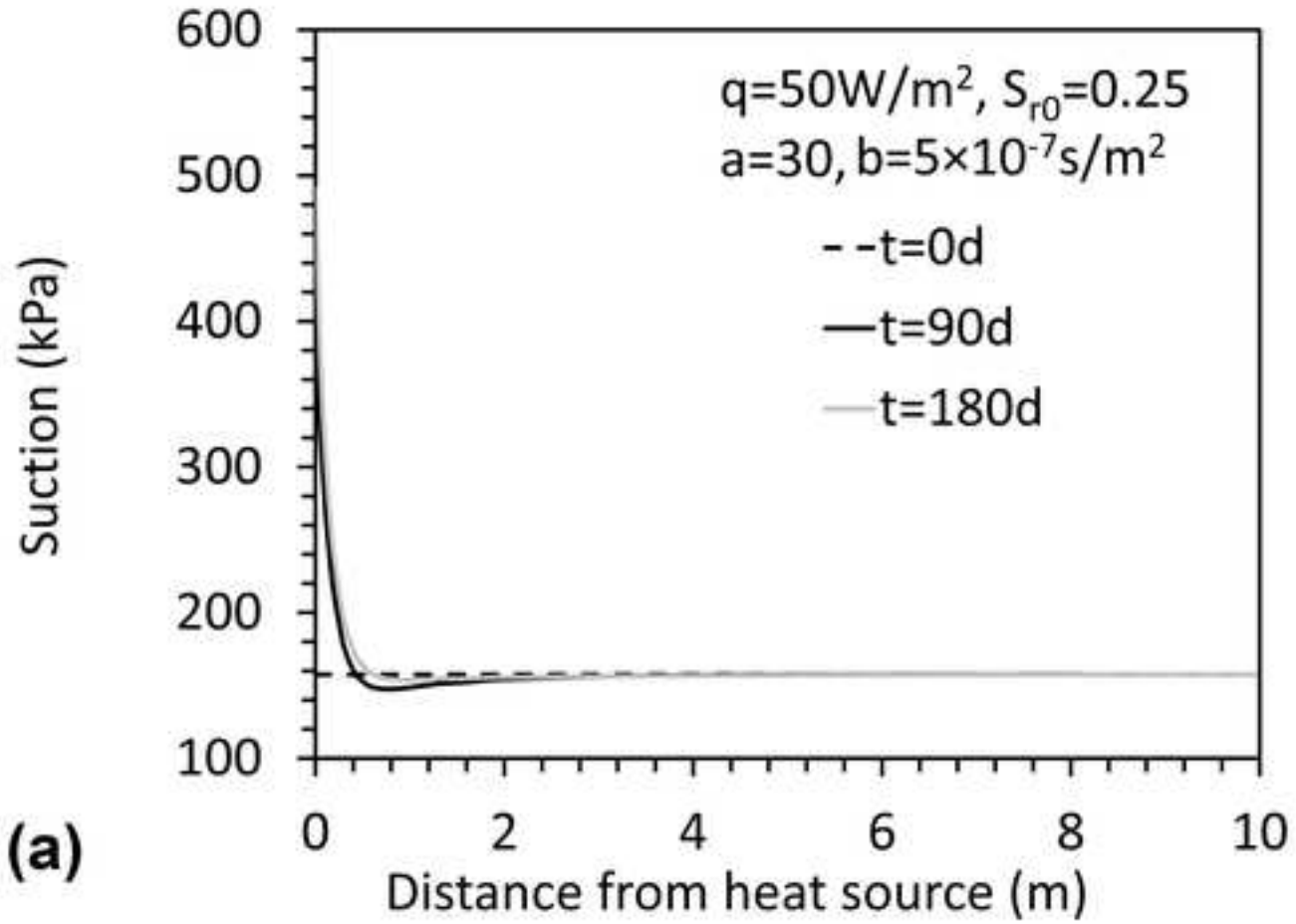

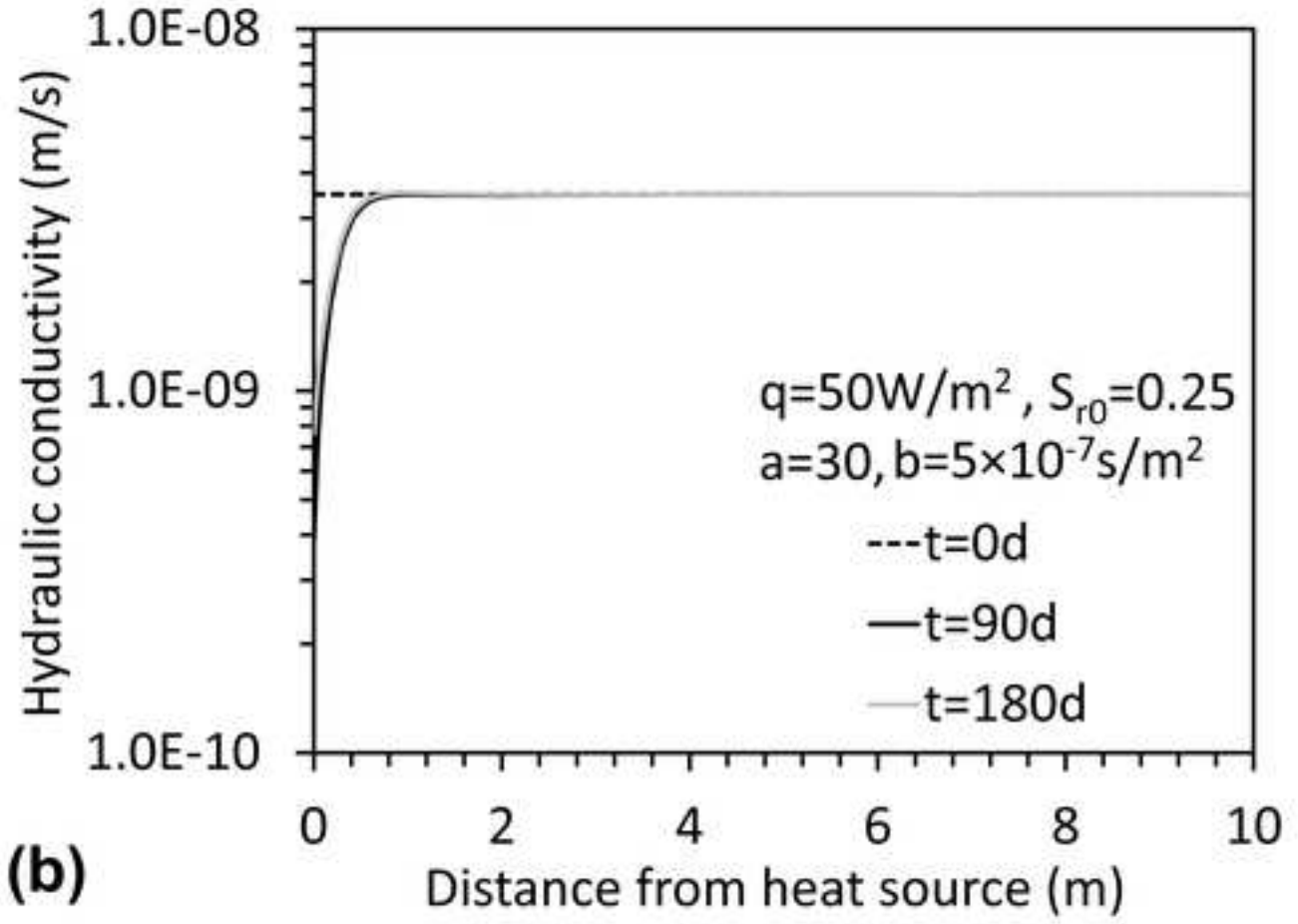

Figure 12

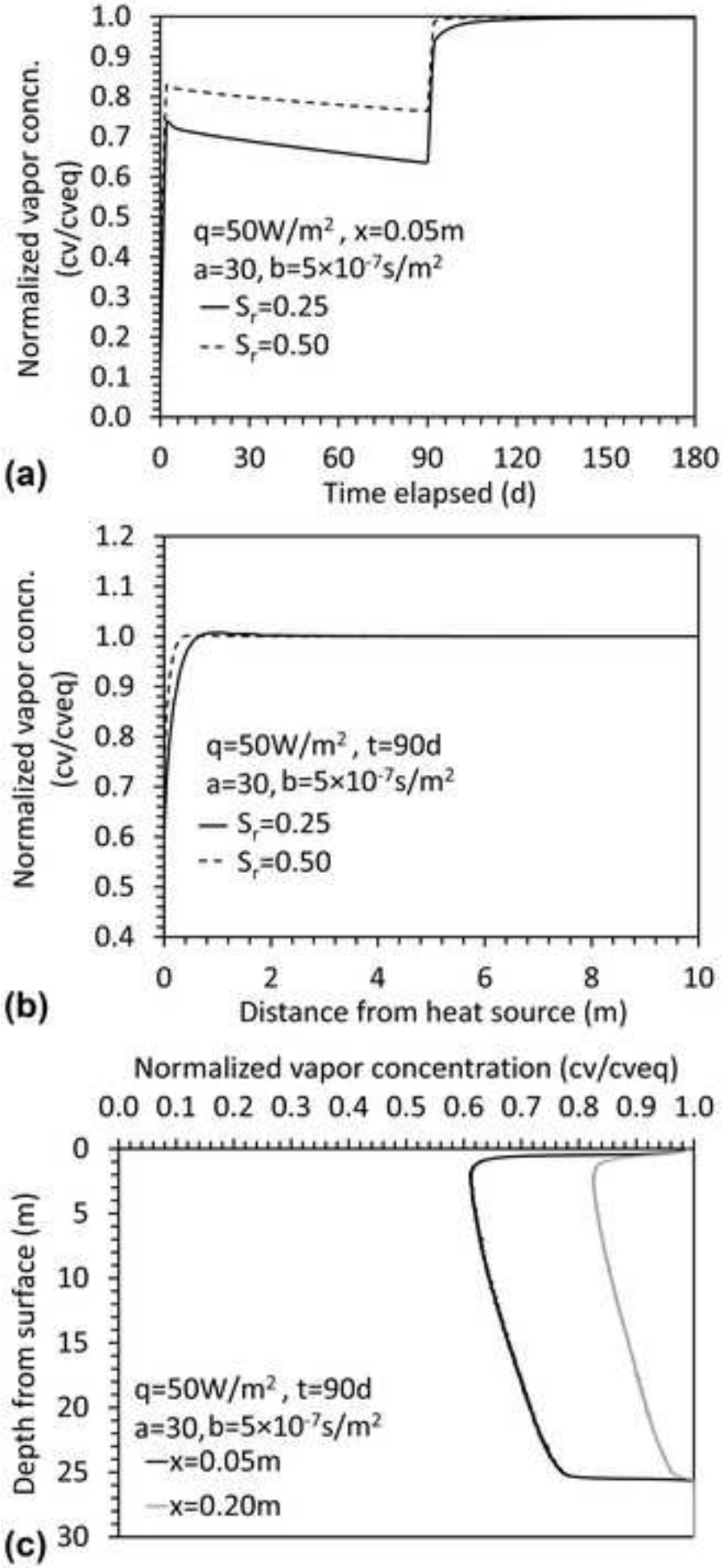

Figure 13

Click here to download Figure Figure 13.tif

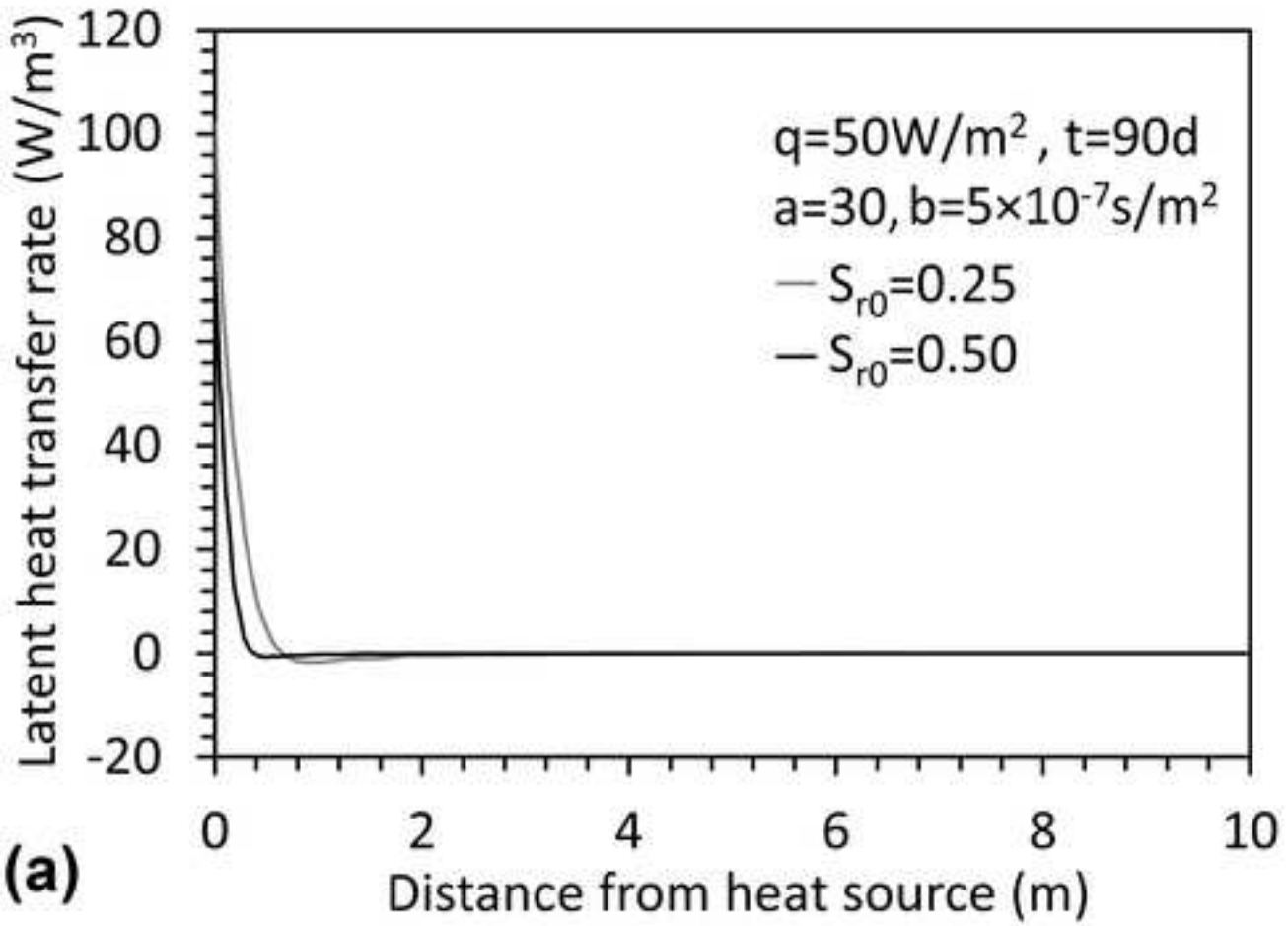

(a)

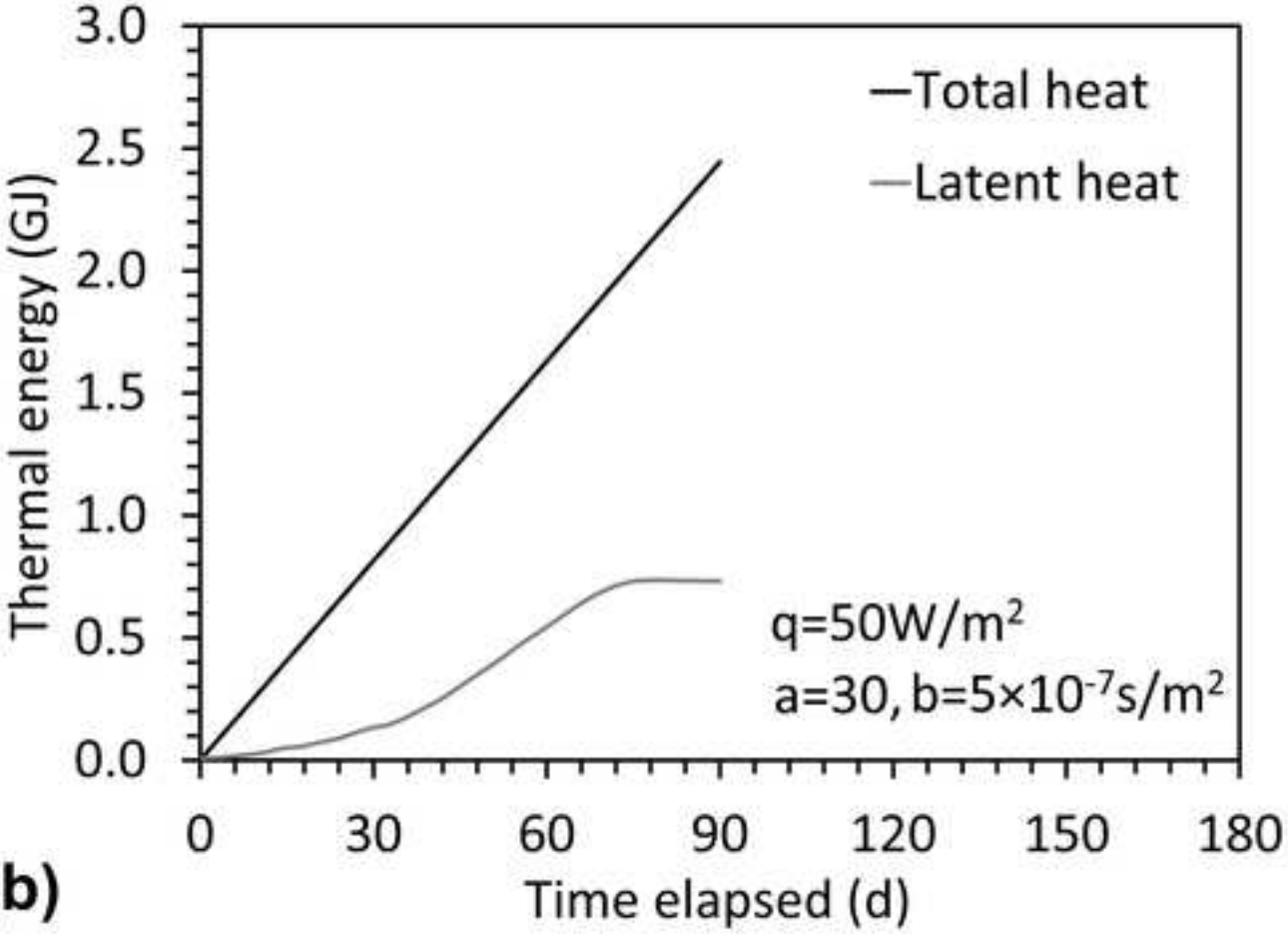

(b)